ARF1 prevents aberrant type I IFN induction by regulating STING activation and recycling

Maximilian Hirschenberger[1], Alice Lepelley[2], Ulrich Rupp[3], Susanne Klute[1], Victoria Hunszinger[1], Lennart Koepke[1], Veronika Merold[4], Blaise Didry-Barca[2], Fanny Wondany[6], Tim Bergner[3], Sebastian Wiese[7], Stefano Volpi[8,9], Marco Gattorno[8], Riccardo Papa[8], Sally-Ann Lynch[10,11], Marte G. Haug[12], Gunnar Houge[13], Kristen M. Wigby[14,15], Jessica Sprague[16], Jerica Lenberg[15], Clarissa Read[3], Paul Walther[3], Jens Michaelis[6], Frank Kirchhoff[1], Carina C. de Oliveira Mann[4], Yanick J. Crow[2,5,*], Konstantin M.J. Sparrer[1,*]

[1]Institute of Molecular Virology, Ulm University Medical Center, 89081 Ulm, Germany
[2]Université Paris Cité, *Imagine* Institute, Laboratory of Neurogenetics and Neuroinflammation, INSERM UMR1163, F-75015, Paris, France
[3]Central Facility for Electron Microscopy, Ulm University, 89081 Ulm, Germany
[4]Institute of Virology, Technical University of Munich, 81675 Munich, Germany
[5]MRC Human Genetics Unit, Institute of Genetics and Cancer, University of Edinburgh, Edinburgh, United Kingdom
[6]Institute of Biophysics, Ulm University, 89081 Ulm, Germany
[7]Core Unit Mass Spectrometry and Proteomics, Ulm University Medical Center, 89081 Ulm, Germany
[8]Centro per le Malattie Autoinfiammatorie e Immunodeficienze, IRCCS Istituto Giannina Gaslini, Genoa, Italy
[9]Universita' degli Studi di Genova, Genoa, Italy
[10]Children's Health Ireland, Crumlin, Dublin, Eire
[11]University College Dublin, Dublin, Eire
[12]Department of Medical Genetics, St. Olav's Hospital, Trondheim, Norway
[13]Department of Medical Genetics, Haukeland University Hospital, 5021 Bergen, Norway
[14]Department of Pediatrics, Division of Genetics, University of California, San Diego, California, USA
[15]Rady Children's Institute for Genomic Medicine, San Diego, California, USA
[16]Division of Pediatric and Adolescent Dermatology, University of California, San Diego, California; Rady Children's Hospital, San Diego

*Address correspondence to: Yanick J. Crow: yanickcrow@mac.com; Konstantin M.J. Sparrer: Konstantin.Sparrer@uni-ulm.de.

RUNNING TITLE: ARF1 regulates STING activation and trafficking

KEYWORDS: ARF1, Interferon, STING, cGAS, Interferonopathy

ABSTRACT

Type I interferon (IFN) signalling is tightly controlled. Upon recognition of DNA by cyclic GMP-AMP synthase (cGAS), stimulator of interferon genes (STING) translocates along the endoplasmic reticulum (ER)-Golgi axis to induce IFN signalling. Termination is achieved through autophagic degradation or recycling of STING by retrograde Golgi-to-ER transport. Here, we identify the GTPase ARF1 as a crucial negative regulator of cGAS-STING signaling. Heterozygous ARF1 missense mutations cause a novel type I interferonopathy associated with enhanced IFN stimulated gene expression. Disease-associated, GTPase-defective, ARF1 results in increased cGAS-STING dependent type I IFN signalling in cell lines and primary patient cells. Mechanistically, mutated ARF1 perturbs mitochondrial fusion causing cGAS activation by aberrant mitochondrial DNA, and promotes accumulation of active STING at the Golgi/ERGIC due to defective retrograde transport. Our data show that ARF1 has an unexpected dual role in maintaining cGAS-STING homeostasis, through the promotion of mitochondrial fusion and STING recycling.

INTRODUCTION

Type I interferon (IFN) mediated innate immunity constitutes an essential element in the response to viral infection, establishing an anti-viral state through the upregulation of hundreds of IFN stimulated genes (ISGs)[1–3]. Contrasting with this protective role against viral infection, inappropriate activation of an IFN response is pathogenic, eventually leading to tissue damage[4]. This dichotomy is particularly well illustrated by the type I interferonopathies, Mendelian diseases characterised by chronically enhanced type I IFN signaling[4,5]. Clinically, these disorders often manifest with neurological features such as encephalopathy, cerebral calcification, leukodystrophy and cerebral atrophy. In addition, extra-neurological involvement can also be seen, with chilblain-like skin lesions a particularly frequent association. Notably, the study of the pathological basis of the type I interferonopathies has provided molecular insight into the induction and regulation of type I IFN signalling in human health and disease[4].

Type I IFNs can be induced through the sensing of foreign viral nucleic acids by innate immune receptors, among them cyclic GMP-AMP synthase (cGAS)[2,6–8]. Notably, cGAS can also be triggered by self-DNA that is erroneously present in the cytoplasm[9]. Upon binding to cytoplasmic DNA, cGAS catalyses the production of a second messenger 2´-3´ cyclic guanosine monophosphate–adenosine monophosphate (cGAMP) from GTP and ATP[6,10]. cGAMP in turn binds to the signalling adaptor stimulator of IFN genes (STING), residing in its inactive form at the endoplasmic reticulum (ER), causing STING to change conformation, oligomerise, and accumulate in the Golgi[7]. Trafficking via the ER-Golgi axis is a major determinant of both STING activation and signal termination[11–13]. Activated STING is transported from the ER to the ER-Golgi intermediate compartment (ERGIC)/Golgi via coatomer protein complex II (COPII) vesicles. At the Golgi/ERGIC, STING recruits Tank binding kinase 1 (TBK1), which in turn activates the transcription factors IRF3 and NF-kB. Both transcription factors eventually

translocate into the nucleus, leading to the induction of type I IFN and other (pro-)inflammatory cytokines. The current model proposes that, after TBK1 activation, STING is transported to the trans-Golgi network (TGN)/Golgi-associated vesicles where it is degraded via the autophagic-lysosomal pathway for signal termination[13]. In addition, increasing evidence suggests that STING can be recycled back to the ER[14–17]. Upon recruitment by Surfeit 4 (SURF4) to coatomer protein complex I (COPI) vesicles, STING is transported in a retrograde manner from the Golgi/ERGIC to the ER, thus also contributing to signal termination[15–17]. COPI trafficking is a highly conserved pathway down to yeast, functioning through the combined action of seven coatomer subunits: α-COP, β-COP, β′-COP, γ-COP, δ-COP, ε-COP, and ζ-COP. Despite these insights, the precise mechanism(s) and key players involved in STING flux and signal termination remain incompletely understood.

Small GTPases are important mediators of intracellular trafficking, among them the family of ADP-ribosylation factors (ARFs) comprising five highly homologous members in humans (ARF1, ARF2/4, ARF3, ARF5 and ARF6)[18]. These molecules have distinct but overlapping roles generally defined by their subcellular localisation[19]. For example, ARF1 is predominantly localised to the cis-Golgi, trans-Golgi and ERGIC[20], whereas ARF6 is present at the plasma membrane[21]. Their major function is to recruit coat proteins, such as COPI components, and mediate budding of transport vesicles from ER/Golgi surfaces. GTPase activity is required for vesicle formation and cargo recruitment by ARF proteins, cycling between a membrane-associated GTP-bound state and a GDP-bound cytoplasmic state[22]. GTPase activity, and GDP to GTP exchange, are regulated by a distinct set of GTPase accelerating proteins (GAP) and guanine nucleotide exchange factors (GEF), respectively, thereby in turn controlling the activity of ARF proteins[22].

Through the characterisation of a novel type I interferonopathy, we have discovered that the small GTPase ARF1 plays a key role in regulating cGAS-STING activity. ARF1 prevents aberrant type

I IFN induction and signalling via a dual mechanism. First, functional ARF1 is required for proper mitochondrial fusion, thus preventing the release and sensing of mitochondrial DNA (mtDNA). In addition, ARF1 mediates retrograde transport of activated STING from the ERGIC/Golgi for signal termination. Mutation of the R99 residue in ARF1 is associated with a type I interferonopathy state, demonstrating attenuated GTPase activity and impaired function. Consequently, mtDNA leaks into the cytoplasm where it triggers cGAS. In addition, signal termination via ER-Golgi trafficking is defective, leading to elevated ISG expression. Our results reveal previously unappreciated roles for ARF1 in cGAS-STING activation and signal termination essential to the maintenance of cellular homeostasis, and provide a mechanistic explanation for a novel auto-inflammatory disease.

RESULTS

Mutations in ARF1 define a novel type I interferonopathy

As part of an ongoing protocol involving the agnostic screening of patients with uncharacterized phenotypes for an upregulation of type I IFN signalling, we identified a patient with skin lesions and significant developmental delay to harbour a *de novo* c.295C>T / p.(R99C) substitution in ARF1 (Supplementary information). His skin disease was consistent with a diagnosis of chilblain lupus, a clinical sign frequently observed in a number of type I interferonopathies including Aicardi-Goutières syndrome (AGS) and STING associated vasculopathy of infancy (SAVI) (Fig. 1a-c). Through Decipher and GeneMatcher/Matchmaker exchange[23], we ascertained two additional patients (RH2003, KW2022) with the same p.(R99C) substitution, in one of whom we could demonstrate that the variant arose *de novo*. Both of these patients exhibited similar skin lesions (Fig. 1d–g), in association with significant developmental delay. We then identified a

123 further patient with a *de novo* c.296G>A / p.(R99H) substitution and a history of cold hands and
124 feet, without frank chilblains (Supplementary information).

125 ARF1 is a small GTPase with a myristylation anchor at the N-terminus that mediates membrane
126 association[22,24]. This is followed by an amphipathic helix and the GTPase domain, consisting of
127 two Switch domains (SW1 and 2) (Fig. 1h). Overall, ARF1 is highly constrained (pLi = 0.9). The
128 arginine at position 99 is conserved from yeast to humans (Fig. 1i and Extended Data Fig. 1a),
129 there are no variants at this residue on gnomAD, and a substitution for a cysteine or histidine is
130 predicted as damaging by *in silico* analyses (Supplementary table 1). Where tested, all (7 of 8)
131 parents were found to be wild type (WT) on both alleles of ARF1 (Extended Data Fig. 1b). Of
132 note, the p.(R99H) substitution was previously reported as a *de novo* mutation in a child with
133 developmental delay and periventricular nodular heterotopia[25]. In Patient 1, we observed increased
134 ISG expression in peripheral blood on the two occasions assayed, and in Patient 2 on the one
135 occasion (Fig. 1j and Supplementary information). IFN signalling status could not be assessed in
136 two other patients.

137 Taken together, these data indicated that mutation of the arginine at position 99 in ARF1 underlays
138 a novel human type I interferonopathy.

139 **ARF1 R99C induces STING-dependent type I IFN activation**

140 To understand the molecular basis of enhanced type I IFN signalling in the context of this novel
141 human type I interferonopathy, we examined the impact of ARF1 R99C expression on innate
142 immune activation. The activity of ARF1 R99C was compared with ARF1 Q71L, which locks the
143 protein in its GTP-bound state, and T31N which is trapped in the GDP-bound state[26]. In HEK293
144 cells stably expressing STING (293-Dual-hSTING-R232), transient expression of ARF1 R99C
145 was sufficient to induce type I IFN signalling in a dose-dependent manner, as assessed by IFN

stimulated response element (ISRE) reporter activity (Fig. 2a, b and Extended Data Fig. 2a). ARF1 Q71L also induced ISRE promoter activity, albeit less robustly than R99C, while ARF1 T31N had only a minor effect. STING was required for induction of type I IFN signalling by ARF1 R99C in HEK293T cells (Fig. 2c and Extended Data Fig. 2b). To avoid triggering high background cGAS-STING dependent responses by plasmid transfection, we then used a lentiviral transduction strategy. Lentivirus-mediated expression of ARF1 R99C in A549-ISRE reporter cells, that naturally express STING and cGAS, resulted in activation of type I IFN signalling (Fig. 2d). These data suggest that endogenous cGAS-STING proteins are sufficient for signalling induction. Expression of WT ARF1 had no effect, compared to treatment with IFN-β and cGAMP used as positive controls. Besides inducing type I IFN via IRF3, cGAS-STING signalling also enhances NF-kB activity[27]. In line with this, expression of ARF1 R99C in A549 cells induced NF-kB signalling (Fig. 2e), whereas expression of ARF1 WT had no effect. Activity of the kinase TBK1 is required downstream of cGAS-STING to activate NF-kB and IRF3[28]. As expected, overexpression of either R99C or Q71L ARF1 in HEK293T cells ectopically expressing cGAS and STING significantly increased the amount of active (i.e. phosphorylated) TBK1 (Fig. 2f, g). Of note, decreased amount of endogenous STING protein upon co-transfection with ARF1 R99C is consistent with STING activation leading to degradation, as observed for STING activation by cGAMP stimulation (Fig. 2e)[13].

To assess these observations in a more physiological setting, we performed experiments using primary human fibroblasts derived from healthy individuals, and from an ARF1-mutated patient. First, primary human lung cells from healthy donors were complemented with ARF1 WT and ARF1 R99C by lentiviral transduction. Only the expression of ARF1 R99C, and exposure to the positive controls cGAMP and IFN-β, resulted in upregulation of ISG mRNAs (OAS1, Mx1) in primary human lung fibroblasts (Fig. 2h, Extended Data Fig. 2c). To determine whether patient-

derived primary fibroblasts release type I IFN, we transferred supernatant from fibroblast cultures of healthy donors (n1 and f1, genotype ARF1 WT) and one patient (#Patient 1, heterozygous ARF1 R99C) on to type I IFN signalling reporter HEK293T cells. Only supernatants from the patient-derived cells resulted in a significant induction of the reporter (Fig. 2i).

Taken together, these results indicate that expression of ARF1 R99C induces a STING-dependent type I IFN response in cell line models and patient-derived primary cells.

Mitochondrial DNA released in the presence of ARF1 R99C triggers cGAS activity

Since the induction of type I IFN signalling by ARF1 R99C was dependent on STING (Fig. 2c), we wondered whether and how cGAS may be involved. Inhibition of cGAS activity using a pharmacological inhibitor, G140, significantly reduced ISRE promoter activation by ARF1 R99C in 293-Dual-hSTING-R232 cells (Extended data Fig. 3a). In line with this, expression of ARF1 WT and R99C via lentiviral transduction in WT and cGAS KO THP-1 monocytes revealed that IFN signalling was only induced in the presence of cGAS (Fig. 3a). As expected, IFN signalling upon stimulation with IFN-β and cGAMP was barely affected. These results suggest that cGAS facilitates type I IFN signalling induced by ARF1 R99C. ARF1 has been reported to regulate mitochondrial homeostasis[29,30]. Thus, we examined whether mutation at R99 may disrupt this function, promoting release of mtDNA, which in turn might activate cGAS[31,32]. Electron microscopy of HEK293T cells revealed mitochondrial disruption in the presence of ARF1 R99C, but not WT ARF1 (Fig. 3b). Indicative of mitochondrial damage, small electron-dense granules were observed in the mitochondria of R99C-expressing cells (Fig. 3b, left panel). With increasing mitochondrial degeneration these granules became larger, and the intermembrane space of the cristae more inflated (Fig. 3b, middle and right panel). To determine the presence of mtDNA in the cytoplasm, we performed fractionation of cells into nuclear, cytoplasmic and mitochondrial

fractions (Fig. 3c). We detected higher levels of mtDNA in the cytoplasm upon overexpression of ARF1 R99C and Q71L compared to WT ARF1 (Fig. 3d). Treatment with ABT-737 and Q-VD-OPH (ABT/QVD), to damage mitochondria and promote mtDNA release[33], was used as a positive control. Notably, in primary fibroblasts of a patient with a heterozygous R99C mutation in ARF1 (#Patient 1), cytoplasmic mtDNA levels were significantly elevated compared to control ARF1 WT donor fibroblasts (n2, f1, I7) (Fig. 3e). Depletion of mtDNA using 2',3' dideoxycytidine (ddC)[34] in U2OS-STING cells reduced the induction of the ISG OAS1 in the presence of ARF1 R99C (Fig. 3f, Extended Data Fig. 3b). In line with this, gene expression of *IFNB1*, *Mx1* and *RSAD2* induced by ARF1 R99C expression was also reduced upon mtDNA depletion (Extended Data Fig. 3d-f). Of note, mtDNA depletion did not change the response to herring testis DNA (HT-DNA) (Extended Data Fig. 3c).

In summary, these data show that expression of ARF1 R99C promotes mitochondrial disruption and leakage of mtDNA into the cytoplasm, and a subsequent induction of ISG expression.

ARF1 R99C destabilizes mitochondria by interfering with mitochondrial fusion

Since ARF1 has been reported to be involved in mitophagy (i.e. autophagic turnover of defective mitochondria), and in the regulation of mitochondrial fusion and fission[29,35], an impairment of either process by ARF1 R99C might cause aberrant mtDNA release via disturbed mitochondrial homeostasis[36–38]. Thus, we explored whether mitophagy is altered by ARF1 R99C, with subsequent impact on mtDNA release. In the presence of both ARF1 WT and R99C, autophagosomes accumulated in HEK293T GFP-LC3B reporter cells (Extended data Fig. 3g). Bafilomycin A1 treatment masked the effect of both ARF1 WT and R99C, suggesting that both proteins reduce autophagosome turnover (Extended data Fig. 3h). Notably, in autophagy-impaired ATG5 KO cells, ARF1 R99C still mediated mtDNA release compared to WT and vector

conditions (Extended data Fig. 3i), suggesting that a defect in autophagy is not responsible for mtDNA release in the presence of ARF1 R99C. Mitotracker staining of mitochondria in transfected HeLa cells revealed a significant reduction in the mitochondrial footprint in the presence of ARF1 R99C (Extended data Fig. 3j, k), indicating mitochondrial fragmentation due to a change in mitochondrial fission or fusion. Analysis of phosphorylated (activation) levels of the mitochondrial fission factor Drp1 revealed no change in the presence of ARF1 R99C (Extended data Fig. 3l). In contrast, the mitochondrial fusion marker mitofusin 1 (MFN1) accumulated significantly in the presence of ARF1 R99C but not ARF1 WT (Fig. 3g). In yeast, ARF1 deficiency leads to Fzo1 (yeast equivalent of MFN1/2) misfolding and aggregation[29]. Thus, accumulation of MFN1 upon ARF1 R99C expression suggests that mitochondrial fusion is impaired. Consistently, ER-mitochondria contacts, that are dependent on proper mitochondrial fusion, were visibly increased (Fig. 3b). To understand whether this impacts mtDNA release by ARF1 R99C, we promoted MFN1 turnover by overexpression of the E3 ubiquitin ligase Valosin Containing Protein (VCP)[29]. Notably, overexpression of VCP reduced mtDNA release induced by ARF1 R99C almost back to basal levels (Fig. 3h, i).

Taken together, these data indicate that ARF1 R99C prevents proper fusion of mitochondria by interfering with MFN1 function, leading to a leakage of mtDNA into the cytoplasm.

Mutation of R99 impairs ARF1 GTPase activity and association with the COPI complex

ARF1 is a small GTPase, and both GTP-GDP cycling and co-factor binding are known to be crucial for its enzymatic activity[18]. Analyses of ARF1 structures, based on PDB: 2J59[39], indicated that residue R99 is not directly involved in binding to GTP or other ARF1 interaction partners. Instead, R99, located on helix α5, forms salt bridges with residue D26, thereby stabilizing the loop β1-α3 which is part of the GTP-binding site of ARF1 (Fig. 4a). D26 is not directly involved in the

coordination of GTP binding (Fig. 4a). However, the correct positioning of the loop β1-α3 is crucial for the stability of ARF1 and GTP hydrolysis[39]. To experimentally assess the effects of the R99C mutation on protein stability, GTP binding and GTP hydrolysis, we purified recombinant ARF1 WT, ARF1 R99C and ARF1 Q71L (Extended Data Fig. 4a), and performed comparative fluorescence thermal shift assays as well as *in vitro* GTPase assays. Both ARF1 WT and R99C proteins bind GTP with similar affinity, as revealed by an increase of the melting temperatures by ~16°C of both proteins in the presence of GTP (Fig. 4b, c). However, a 15°C lower melting temperature of ARF1 R99C compared to ARF1 WT or ARF1 Q71L, indicates reduced conformational stability (Extended Data Fig. 4b). Consequently, the *in vitro* GTPase activity of ARF1 R99C was significantly lower than that of WT ARF1 (Fig. 4d). Of note, reduced conformational stability does not lead to low expression levels of ectopically expressed R99C ARF1, which would be indicative of an unstable protein (Figs. 2-4). Additionally, ARF1 dimerization, known to be required for vesicle transport activity and GTP hydrolysis[18,40], was similar between mutant and WT ARF1 (Extended Data Fig. 4c). To promote the GTPase activity of ARF1 R99C, we co-expressed mutant ARF1 with the ARF1 GTPase activating protein (GAP) ARFGAP1, and with the GTP exchange factor (GEF) BIG1[22]. Accelerating GTPase activity by a GAP, or increasing GDP/GTP exchange by a GEF, rescued aberrant type I IFN induction by ARF1 R99C in 293-Dual-hSTING-R232 cells (Fig. 4e).

Destabilization of ARF1 may also result in decreased binding to important effectors and co-factors. To explore this possibility, we performed stable isotope labelling of amino acids in cell culture (SILAC) mass spectrometry experiments, comparing the interaction of endogenous proteins to either ARF1 WT or ARF1 R99C expressed in HEK293T cells, in heavy and light arginine containing media, respectively (Extended Data Fig. 4d). Proteins were purified while maintaining endogenous interaction partners (Extended Data Fig. 4e), and ~1900 co-purified proteins were

identified by mass spectrometry analysis of the lysates (Supplementary table 2, Fig. 4f). Notably, all major protein components of COPI complex (COPA, COPB1, COPB2, COPD/ARCN1, COPE, COPG1, COPG2 and COPS8) showed on average a ~3400-fold lower association with ARF1 R99C. Panther DB aided Gene Ontology (GO) term analysis of the top 100 proteins binding with lower affinity to ARF1 R99C confirmed that interaction with proteins of the COPI pathway was significantly affected (GoTerm: COPI vesicle coat (GO:0030126), >100-fold (maximum) downregulation, p = 4.85E-12; COPI-coated vesicle membrane (GO:0030663), 76.99-fold downregulation, p = 2.94E-11; COPI-coated vesicle (GO:0030137), 62.99-fold downregulation, p = 9.41E-11) (Fig. 4g).

Altogether, biochemical characterization revealed that R99C reduced conformational stability, GTPase activity and association with components of the COPI complex of ARF1.

ARF1 is required for retrograde transport from the ERGIC to the ER

To understand whether the reduced association of ARF1 R99C with components of the COPI transport machinery might affect STING trafficking and signaling directly, we sought to activate STING independently of cGAS. Indeed, bypassing the requirement for cGAS by treatment with cGAMP showed that ARF1 R99C further enhances IFN signaling compared to WT ARF1 (Fig. 5a, b). Consistently, we observed elevated IFN signalling in the presence of ARF1 R99C upon expression of an active STING mutant (R238A/Y240A) that does not bind or require cGAMP[41,42] (Fig. 5c). As expected, STING with a mutation in S366A, that is unable to bind to TBK1, did not induce type I IFN signaling, despite being expressed at similar levels to WT STING (Extended Data Fig. 5b). Neither ARF1 WT nor R99C caused further signaling activation. The above results suggest that, in addition to dysfunction of ARF1 in limiting mtDNA leakage to the cytoplasm, ARF1 R99C also enhances type I IFN signalling through changes in STING trafficking and

signalling downstream of cGAS/cGAMP. As STING recycling has been proposed to occur by retrograde transport via COPI vesicles[14–17], we then asked if the decreased association of ARF1 R99C with COPI vesicles might result in decreased STING recycling, and thus impaired signal termination of STING and prolonged IFN induction. To this end, we explored the impact of patient-associated mutant ARF1 on retrograde Golgi/ERGIC-ER transport. Electron microscopy analysis revealed that ARF1 R99C expression led to altered Golgi/ERGIC structures, whereas empty vector or ARF1 WT transfection had no effect (Fig. 5d). Indeed, scanning-transmission-electron-microscopy (STEM) tomography analysis revealed that, in the presence of ARF1 R99C, the volume density of the lumen of the Golgi is increased (Fig. 5e), whereas the volume density of vesicles released from the Golgi and the ER is significantly reduced compared to ARF1 WT (Fig. 5f). Focusing on the ERGIC, confocal microscopy analysis confirmed the alteration of Golgi structure. Specifically, it showed that the number of ERGIC-53 positive vesicles per cell i.e. ERGIC vesicles, was significantly reduced in the presence of ARF1 R99C and ARF1 Q71L (Fig. 5g, left panel, Extended Data Fig. 5c). Conversely, the area occupied by individual ERGIC-53 positive structures was increased upon ARF1 R99C and Q71L expression (Fig. 5g, middle panel), while the total area of the ERGIC-53 positive structures per cell did not change (Fig. 5g, right panel). Thus, in the presence of ARF1 R99C, fewer but larger vesicles/ERGIC structures are present, suggesting impaired budding of vesicles from the ERGIC. To examine whether ARF1 R99C impacts general ERGIC to ER trafficking, we used a thermolabile VSV-G protein fused to the KDEL retrograde trafficking signal[43]. Upon decreasing the temperature to 32°C, the normally ER-resident construct is transported to the Golgi, while shifting to 40°C partially unfolds VSV-G thereby inducing retrograde transport back to the ER. Both ARF1 WT and R99C expression did not impact VSV-G increased co-localisation with the cis-Golgi (marker GM130) upon lowering the temperature (Fig. 5h, Extended Data Fig. 5d). However, when raising the temperature to 40°C,

retrograde transport was almost completely abrogated in the presence of ARF1 R99C, but unaffected by ARF1 WT expression (Fig. 5h).

In summary, the above data demonstrate that ARF1 R99C causes a defect in Golgi-ER retrograde trafficking and reduced vesicular budding from the Golgi/ERGIC.

Active STING is trapped at the Golgi/ERGIC by ARF1 R99C

To examine the consequences of defective retrograde transport on STING in the presence of ARF1 R99C, we examined the co-localisation of ARF1 and STING-eGFP in HeLa cells relative to endogenous markers of the Golgi network (Fig. 6a-f, Extended Data Fig. 6a-c). As controls, ARF1 Q71L is expected to show increased membrane association with the Golgi/ERGIC, whereas ARF1 T31N is thought to be more cytoplasmic[18]. While ARF1 WT, R99C and Q71L localised similarly to the cis-Golgi as revealed by co-localisation with GM130, ARF1 T31N showed a reduced co-localisation with GM130 (Fig. 6a, b). Notably, expression of both ARF1 R99C and Q71L led to a significant increase of eGFP-STING localization at the cis-Golgi signal compared to WT and T31N ARF1 (Fig. 6a, c). Analysis of ERGIC localisation revealed that ARF1 R99C and Q71L showed markedly increased co-localisation with the ERGIC compared to ARF1 WT (Extended Data Fig. 6a-c). Consistent with this, expression of ARF1 R99C and Q71L significantly increased the co-localisation between eGFP-STING and ERGIC-53, whereas ARF1 WT and T31N had little or no impact on STING localisation at the ERGIC (Extended Data Fig. 6a-c). The presence of ARF1 R99C did not alter the localization of eGFP-STING with respect to the trans-Golgi network (TGN46) (Extended Data Fig. 6d-f). In primary fibroblasts from a healthy donor (genotype ARF1 WT), endogenous STING only accumulates at the Golgi network (GM130) upon stimulation with cGAMP (Fig. 6d, e). In contrast, in fibroblasts from a patient heterozygous for the R99C mutation in ARF1 (#Patient 1), STING accumulated at the cis-Golgi/ERGIC even in the absence of cGAMP stimulation. This is consistent with the data from our cell line experiments (Fig. 6d, e). To analyze

the effect of ARF1 mutants on the localization of endogenous STING in more detail, we employed super-resolution microscopy (stimulated emission/depletion microscopy, STED). Two colour STED microscopy in primary human lung fibroblasts transduced with empty, ARF1 WT or ARF R99C expressing lentiviruses confirmed that, in the presence of ARF1 R99C, endogenous STING accumulates at/around the cis-Golgi (GM130) network (exemplary image in Fig. 6f, further images in Extended Data Fig. 6g).

To determine whether STING accumulates in its active state at the Golgi/ERGIC, we co-stained phospho-TBK1 (p-S172) as a marker of STING activity *in situ*. Confocal analysis revealed that in the presence of transduced ARF1 R99C, but not ARF1 WT, increased amounts of activated TBK1 were present in the proximity of the ERGIC in primary human lung fibroblasts (Fig. 6g, h).

Taken together, these results suggest that ARF1 plays a role in the retrograde transport of STING from the Golgi/ERGIC to the ER. When trafficking is affected due to impaired ARF1 GTPase activity (e.g. by mutations at R99C or Q71L), STING accumulates at the cis-Golgi/ERGIC in both cell models and primary cells isolated from patients, leading to activation of TBK1 and sustained IFN induction/signalling.

DISCUSSION

The avoidance of chronic activation of a type I IFN response is fundamental to immunological homeostasis[4]. Engagement of the cGAS-STING pathway occurs through the recognition of DNA by cGAS (‘Trigger’), and subsequent trafficking of STING from the ER to the Golgi. To terminate such signalling, STING is transported back to the ER (‘Recycling’) and degraded via autophagy (‘Removal’). Through an analysis of the function of an ARF1 mutant associated with elevated IFN signalling *in vivo,* we have identified a previously unrecognised dual role of the GTPase ARF1 in both preventing aberrant cGAS activation and promoting signal termination by the recycling of

STING (Extended Data Fig 7). We show that functional ARF1 promotes proper mitochondrial fusion, thereby preventing aberrant stimulation of cGAS by mtDNA. In addition, we demonstrate a role for ARF1 in the termination of cGAS-STING signalling, by facilitating COPI vesicle-mediated trafficking of STING from the ERGIC to the ER. When the GTPase activity of ARF1 is impaired, either by disease-associated mutations at R99 or by the characterised GTP-locked Q71L mutation, type I IFN responses are enhanced. Consequently, patients bearing a heterozygous R99 mutation in ARF1 manifest features of chronic innate immune activation.

Complete disruption (e.g. by drugs such as Brefeldin A) or depletion of ARF1 is well known to decrease STING-dependent signalling[11,12,44]. This effect is most likely due to a generalised disturbance of the Golgi structure/transporting system[45], including the anterograde transport of STING required for its activation. In contrast, our investigation of a physiologically relevant human interferonopathy-associated ARF1 mutant has allowed us to define an ARF1-specific effect on retrograde STING trafficking thus differentiating it from a non-specific effect on anterograde transport.

GTPases are core components involved in the regulation of mitochondrial fission and fusion that include MFN1, MFN2, and OPA1. A role of ARF1 in regulating Fzo1 (the yeast MFN1 homologue) was previously proposed in yeast[46]. In the absence of functional ARF1, Fzo1 accumulated, leading to a loss of mitochondrial fusion. Our data show that human ARF1 also regulates mitochondrial fusion. Thus, non-functional ARF1 leads to impaired mitochondrial integrity and aberrant accumulation of MFN1. The human homologue of yeast Fzo1 associated E3 ubiquitin ligase cdc48, VCP, was able to resolve the mitochondrial fusion impairment consequent upon defective ARF1. These data suggest that ARF1 plays an important role in mitochondrial fusion and fission in mammals. Of note, it was recently shown that Golgi-derived vesicles may aid mitochondrial fusion and fission, spatially linking ARF1 and mitochondria[30,47].

Previous work has shown that defects in retrograde transport can mediate chronic type I IFN release in a cGAS dependent[17] or independent fashion[14]. Our mechanistic analyses indicate that IFN induction in patients with ARF1 R99C is dependent on cGAS activity. Given impaired mitochondrial integrity in both model and patient cells, our data suggest that, even in the absence of a pathogen-derived cGAS trigger, ARF1 dysfunction may lead to sterile inflammation. The relative contribution of defects in mitochondrial maintenance and retrograde transport of STING to an ARF1-dependent type I interferonopathy disease-state remains to be determined. Although each process may be sufficient to cause disease[14,15,48], it is possible that these two aberrant activities drive the mutant-associated phenotype synergistically, i.e. stimulation of the cGAS-STING pathway via mtDNA is further exacerbated by defective signal termination. Improper termination of cGAS-STING triggering in the presence of ARF1 R99C, e.g. after exogenous triggers like viral infection, might accelerate and aggravate disease progression. Future studies dissecting the different functions of ARF1 in the regulation of the IFN response to infectious diseases, and the molecular mechanism by which ARF1 maintains mitochondrial integrity, are warranted.

Our data add to the emerging evidence that impaired control of cGAS-STING signal activation and termination is central to the pathogenesis of a number of type I interferonopathies[4]. The first described example of a Mendelian disease associated with chronic type I IFN signalling was Aicardi–Goutières syndrome (AGS). Mutations in TREX1, the RNase H2 complex, the deoxynucleoside triphosphate triphosphohydrolase SAMHD1 and the U7 small nuclear RNP complex all result in IFN induction by self DNA[4]. Recently, we described pathogenic mutations in mitochondrial ATPase family AAA domain-containing protein 3A (ATAD3A) to result in a leakage of mtDNA into the cytosol[48]. Furthermore, defects in STING trafficking along the ER-Golgi axis have been reported to underlie various type I interferonopathy diseases. For example, activating mutations in STING cause SAVI[49–51], where *in vitro* studies revealed that mutations in

the oligomerisation interface of STING (e.g. N154S, V155M and V147L, G207E, R281Q, R284G and R284S) result in spontaneous cGAMP-independent accumulation of STING at the Golgi, and aberrant induction of type I IFN signalling. Related to this, dysregulation of STING retrieval from the Golgi, due to heterozygous missense mutations in a component of COPI, coatomer protein subunit alpha (COPA), lead to enhanced type I IFN signalling[14,15,52]. Here, STING has been suggested to be recruited to COPA-containing COPI vesicles via SURF4[15,17], although other players may also be involved in regulating and triggering retrograde transport of STING. Besides recycling as a mechanism of signal termination, active STING is captured for subsequent autophagy-dependent degradation[11,13,53]. Recently, it was shown that ARF1 may also have a role in autophagy. However, our data show that cGAS-STING activation by the ARF1 R99C mutation is not mediated by autophagy[54]. Future studies are needed to genetically dissect the relative contribution of autophagy-mediated STING turnover and ARF1-mediated STING recycling to overall cGAS/STING signal termination.

Our data indicate a general defect in retrograde trafficking in the presence of ARF1 R99C (Fig. 5g, h). Besides STING recycling, retrograde trafficking retrieves key factors required for ER export[55,56], and is central to ER and Golgi homeostasis[57]. It is possible that non-IFN mediated mechanisms also contribute to the disease phenotype reported here. That being said, the recording of elevated levels of ISGs in patient blood, and the skin lesions present in three of the four cases that we ascertained (Fig. 1), are highly characteristic of other Mendelian type I interferonopathies[4,5]. Some functions of ARF1 are redundant and may be compensated by other ARF proteins[55,58,59]. However, any such compensation is clearly insufficient in the case of the heterozygous mutations at R99 of ARF1. We speculate that homozygous spontaneous mutations of ARF1 would not be viable. Of note, similar to other interferonopathies with a defect in STING trafficking, such as the COPA syndrome, one defective allele is sufficient for disease[14]. Thus,

ARF1 R99C and other disease-causing mutations in the STING trafficking pathway may act in a dominant negative fashion in regards to DNA sensing, while the heterozygous presence of WT ARF1 may be sufficient to maintain organismal viability.

In summary, through an exploration of the mechanistic basis of a novel human type I interferonopathy, our data establish key roles of the small GTPase ARF1 in both ensuring mitochondrial fusion and in Golgi-ER retrograde STING trafficking to prevent aberrant cGAS-STING pathway activity. These data highlight the importance of recycling mechanisms in innate immune homeostasis, and provide first evidence towards involvement of Golgi-associated ARF GTPases in mitochondrial integrity. Further, our results may inform a targeted treatment approach to the ARF-dependent type I interferonopathy state.

ACKNOWLEDGEMENTS

We thank Jana-Romana Fischer, Birgit Ott, Regina Burger, Daniela Krnavek, Kerstin Regensburger, Martha Meyer and Nicola Schrott for excellent technical assistance. This study was supported by DFG (German Research Foundation) grants SP1600/4-1 (to KMJS), SPP1923 (to KMJS and FK), CRC1279 (to KMJS, FK, JM, CR, SW and PW), as well as the BMBF to FK (Restrict SARS-CoV-2) and KMJS (IMMUNOMOD) and Emmy Noether Programme 458004906 to CCOM. YJC sincerely thanks Mathieu Rodero, Tatiana Moreau, Elizabeth Sztul and Paul Randazzo for the generation of early preliminary data not included in the manuscript, and Marine Depp and Carolina Uggenti for providing the eGFP-STING plasmid. YJC also thanks Paolo Piccolo for expert clinical phenotyping, Ignazia Prigione for experimental support, Gillian Rice for deriving interferon scores, and Jean-Madeleine de Sainte Agathe for clinical advice. YJC acknowledges the European Research Council (786142 E-T1IFNs), a state subsidy from the

Agence Nationale de la Recherche (France) under the 'Investissements d'avenir' program bearing the reference ANR-10-IAHU-01, and MSDAVENIR (Devo-Decode Project). This study makes use of data generated by the DECIPHER community, with a full list of contributing centres available at http://decipherge nomics.org/about/ stats and via email from contact@deciphergenomics.org. Funding for the DECIPHER project was provided by the Wellcome Trust. AL acknowledges Inserm International Research Project (Inserm IRP) program. MH, LK, SK and VH are part of the international graduate school in molecular medicine, Ulm (IGradU).

AUTHOR CONTRIBUTIONS

YJC, AL, MH and KMJS conceived the project, and designed and interpreted experiments. MH performed most of the experiments. AL, VH, LK, SK, VM, BDB performed additional experiments. UR, TB, CR and PW contributed the electron microscopy studies. FW and JM provided superresolution imaging. VM and CCdOM performed and planned the *in vitro* experiments. CCdOM, JM, FK supervised experiments and helped interpret data. SV, MG, RP, SAL, MGH, GH, KMW, JS, JL contributed patient data. YJC, AL, MH and KMJS wrote the manuscript.

DECLARATIONS OF INTERESTS

All authors declare no competing interests.

REFERENCES

1. Schoggins, J. W. Interferon-Stimulated Genes: What Do They All Do? *Annu. Rev. Virol.* **6**, 567–584 (2019).
2. Sparrer, K. M. J. & Gack, M. U. Intracellular detection of viral nucleic acids. *Curr. Opin. Microbiol.* **26**, 1–9 (2015).

3. Koepke, L., Gack, M. U. & Sparrer, K. M. The antiviral activities of TRIM proteins. *Curr. Opin. Microbiol.* **59**, 50–57 (2021).
4. Crow, Y. J. & Stetson, D. B. The type I interferonopathies: 10 years on. *Nat. Rev. Immunol.* 1–13 (2021) doi:10.1038/s41577-021-00633-9.
5. Crow, Y. J. Type I interferonopathies: a novel set of inborn errors of immunity. *Ann. N. Y. Acad. Sci.* **1238**, 91–98 (2011).
6. Ablasser, A. & Chen, Z. J. cGAS in action: Expanding roles in immunity and inflammation. *Science* **363**, eaat8657 (2019).
7. Hopfner, K.-P. & Hornung, V. Molecular mechanisms and cellular functions of cGAS-STING signalling. *Nat. Rev. Mol. Cell Biol.* **21**, 501–521 (2020).
8. Sun, L., Wu, J., Du, F., Chen, X. & Chen, Z. J. Cyclic GMP-AMP Synthase is a Cytosolic DNA Sensor that Activates the Type-I Interferon Pathway. *Science* **339**, (2013).
9. Gao, D. *et al.* Activation of cyclic GMP-AMP synthase by self-DNA causes autoimmune diseases. *Proc. Natl. Acad. Sci.* **112**, E5699–E5705 (2015).
10. Wu, J. *et al.* Cyclic GMP-AMP is an endogenous second messenger in innate immune signaling by cytosolic DNA. *Science* **339**, 826–830 (2013).
11. Gui, X. *et al.* Autophagy induction via STING trafficking is a primordial function of the cGAS pathway. *Nature* **567**, 262–266 (2019).
12. Dobbs, N. *et al.* STING Activation by Translocation from the ER Is Associated with Infection and Autoinflammatory Disease. *Cell Host Microbe* **18**, 157–168 (2015).
13. Gonugunta, V. K. *et al.* Trafficking-Mediated STING Degradation Requires Sorting to Acidified Endolysosomes and Can Be Targeted to Enhance Anti-tumor Response. *Cell Rep.* **21**, 3234–3242 (2017).

14. Lepelley, A. *et al.* Mutations in COPA lead to abnormal trafficking of STING to the Golgi and interferon signaling. *J. Exp. Med.* **217**, e20200600 (2020).
15. Deng, Z. *et al.* A defect in COPI-mediated transport of STING causes immune dysregulation in COPA syndrome. *J. Exp. Med.* **217**, e20201045 (2020).
16. Steiner, A. *et al.* Deficiency in coatomer complex I causes aberrant activation of STING signalling. *Nat. Commun.* **13**, 2321 (2022).
17. Mukai, K. *et al.* Homeostatic regulation of STING by retrograde membrane traffic to the ER. *Nat. Commun.* **12**, 61 (2021).
18. Bento, C. F., Puri, C., Moreau, K. & Rubinsztein, D. C. The role of membrane-trafficking small GTPases in the regulation of autophagy. *J. Cell Sci.* **126**, 1059–1069 (2013).
19. Pennauer, M., Buczak, K., Prescianotto-Baschong, C. & Spiess, M. Shared and specific functions of Arfs 1-5 at the Golgi revealed by systematic knockouts. *J. Cell Biol.* **221**, e202106100 (2022).
20. Kahn, R. A. Toward a model for Arf GTPases as regulators of traffic at the Golgi. *FEBS Lett.* **583**, 3872–3879 (2009).
21. Aikawa, Y. & Martin, T. F. J. ARF6 regulates a plasma membrane pool of phosphatidylinositol(4,5)bisphosphate required for regulated exocytosis. *J. Cell Biol.* **162**, 647–659 (2003).
22. Sztul, E. *et al.* ARF GTPases and their GEFs and GAPs: concepts and challenges. *Mol. Biol. Cell* **30**, 1249–1271 (2019).
23. Sobreira, N., Schiettecatte, F., Valle, D. & Hamosh, A. GeneMatcher: a matching tool for connecting investigators with an interest in the same gene. *Hum. Mutat.* **36**, 928–930 (2015).
24. Goldberg, J. Structural basis for activation of ARF GTPase: mechanisms of guanine nucleotide exchange and GTP-myristoyl switching. *Cell* **95**, 237–248 (1998).

25. Ge, X. *et al.* Missense-depleted regions in population exomes implicate ras superfamily nucleotide-binding protein alteration in patients with brain malformation. *NPJ Genomic Med.* **1**, 16036 (2016).

26. Dascher, C. & Balch, W. E. Dominant inhibitory mutants of ARF1 block endoplasmic reticulum to Golgi transport and trigger disassembly of the Golgi apparatus. *J. Biol. Chem.* **269**, 1437–1448 (1994).

27. Ishikawa, H. & Barber, G. N. STING is an endoplasmic reticulum adaptor that facilitates innate immune signalling. *Nature* **455**, 674–678 (2008).

28. Yum, S., Li, M., Fang, Y. & Chen, Z. J. TBK1 recruitment to STING activates both IRF3 and NF-κB that mediate immune defense against tumors and viral infections. *Proc. Natl. Acad. Sci.* **118**, e2100225118 (2021).

29. Ackema, K. B. *et al.* The small GTPase Arf1 modulates mitochondrial morphology and function. *EMBO J.* **33**, 2659–2675 (2014).

30. Nagashima, S. *et al.* Golgi-derived PI(4)P-containing vesicles drive late steps of mitochondrial division. *Science* **367**, 1366–1371 (2020).

31. Huang, L. S. *et al.* mtDNA Activates cGAS Signaling and Suppresses the YAP-Mediated Endothelial Cell Proliferation Program to Promote Inflammatory Injury. *Immunity* **52**, 475-486.e5 (2020).

32. West, A. P. *et al.* Mitochondrial DNA stress primes the antiviral innate immune response. *Nature* **520**, 553–557 (2015).

33. White, M. J. *et al.* Apoptotic Caspases Suppress mtDNA-Induced STING-Mediated Type I IFN Production. *Cell* **159**, 1549–1562 (2014).

34. Nelson, I., Hanna, M. G., Wood, N. W. & Harding, A. E. Depletion of mitochondrial DNA by ddC in untransformed human cell lines. *Somat. Cell Mol. Genet.* **23**, 287–290 (1997).

35. Rabouille, C. Old dog, new tricks: Arf1 required for mitochondria homeostasis. *EMBO J.* **33**, 2604–2605 (2014).

36. Rai, P. *et al.* IRGM1 links mitochondrial quality control to autoimmunity. *Nat. Immunol.* **22**, 312–321 (2021).

37. Willemsen, J. *et al.* TNF leads to mtDNA release and cGAS/STING-dependent interferon responses that support inflammatory arthritis. *Cell Rep.* **37**, 109977 (2021).

38. Bao, D. *et al.* Mitochondrial fission-induced mtDNA stress promotes tumor-associated macrophage infiltration and HCC progression. *Oncogene* **38**, 5007–5020 (2019).

39. Ménétrey, J. *et al.* Structural basis for ARF1-mediated recruitment of ARHGAP21 to Golgi membranes. *EMBO J.* **26**, 1953–1962 (2007).

40. Brumm, S. *et al.* Coordinated Activation of ARF1 GTPases by ARF-GEF GNOM Dimers Is Essential for Vesicle Trafficking in Arabidopsis. *Plant Cell* **32**, 2491–2507 (2020).

41. Li, S. *et al.* Prolonged activation of innate immune pathways by a polyvalent STING agonist. *Nat. Biomed. Eng.* **5**, 455–466 (2021).

42. He, Y. *et al.* Self-assembled cGAMP-STINGΔTM signaling complex as a bioinspired platform for cGAMP delivery. *Sci. Adv.* **6**, eaba7589 (2020).

43. Cole, N. B., Ellenberg, J., Song, J., DiEuliis, D. & Lippincott-Schwartz, J. Retrograde Transport of Golgi-localized Proteins to the ER. *J. Cell Biol.* **140**, 1–15 (1998).

44. Decout, A., Katz, J. D., Venkatraman, S. & Ablasser, A. The cGAS–STING pathway as a therapeutic target in inflammatory diseases. *Nat. Rev. Immunol.* **21**, 548–569 (2021).

45. Wood, S. A., Park, J. E. & Brown, W. J. Brefeldin A causes a microtubule-mediated fusion of the trans-Golgi network and early endosomes. *Cell* **67**, 591–600 (1991).

46. Ackema, K. B. *et al.* The small GTPase Arf1 modulates mitochondrial morphology and function. *EMBO J.* **33**, 2659–2675 (2014).

47. Rasmussen, M. L., Robertson, G. L. & Gama, V. Break on Through: Golgi-Derived Vesicles Aid in Mitochondrial Fission. *Cell Metab.* **31**, 1047–1049 (2020).

48. Lepelley, A. *et al.* Enhanced cGAS-STING-dependent interferon signaling associated with mutations in ATAD3A. *J. Exp. Med.* **218**, e20201560 (2021).

49. Frémond, M.-L. *et al.* Overview of STING-Associated Vasculopathy with Onset in Infancy (SAVI) Among 21 Patients. *J. Allergy Clin. Immunol. Pract.* **9**, 803-818.e11 (2021).

50. Jeremiah, N. *et al.* Inherited STING-activating mutation underlies a familial inflammatory syndrome with lupus-like manifestations. *J. Clin. Invest.* **124**, 5516–5520 (2014).

51. Liu, Y. *et al.* Activated STING in a Vascular and Pulmonary Syndrome. *N. Engl. J. Med.* **371**, 507–518 (2014).

52. Watkin, L. B. *et al.* COPA mutations impair ER-Golgi transport causing hereditary autoimmune-mediated lung disease and arthritis. *Nat. Genet.* **47**, 654–660 (2015).

53. Prabakaran, T. *et al.* Attenuation of cGAS-STING signaling is mediated by a p62/SQSTM1-dependent autophagy pathway activated by TBK1. *EMBO J.* **37**, e97858 (2018).

54. Jia, M. *et al.* Myristic acid as a checkpoint to regulate STING-dependent autophagy and interferon responses by promoting N-myristoylation. *Nat. Commun.* **14**, 660 (2023).

55. Adarska, P., Wong-Dilworth, L. & Bottanelli, F. ARF GTPases and Their Ubiquitous Role in Intracellular Trafficking Beyond the Golgi. *Front. Cell Dev. Biol.* **9**, (2021).

56. Gilbert, C. E., Sztul, E. & Machamer, C. E. Commonly used trafficking blocks disrupt ARF1 activation and the localization and function of specific Golgi proteins. *Mol. Biol. Cell* **29**, 937–947 (2018).

57. Spang, A. Retrograde Traffic from the Golgi to the Endoplasmic Reticulum. *Cold Spring Harb. Perspect. Biol.* **5**, a013391 (2013).

593 58. Nakai, W. *et al.* ARF1 and ARF4 regulate recycling endosomal morphology and retrograde
594 transport from endosomes to the Golgi apparatus. *Mol. Biol. Cell* **24**, 2570–2581 (2013).
595 59. Sumiyoshi, M. *et al.* Arf1 and Arf6 Synergistically Maintain Survival of T Cells during
596 Activation. *J. Immunol.* **206**, 366–375 (2021).
597 60. Presley, J. F. *et al.* ER-to-Golgi transport visualized in living cells. *Nature* **389**, 81–85
598 (1997).
599 61. Hayn, M. *et al.* Systematic functional analysis of SARS-CoV-2 proteins uncovers viral
600 innate immune antagonists and remaining vulnerabilities. *Cell Rep.* **35**, 109126 (2021).
601 62. Koepke, L. *et al.* An improved method for high-throughput quantification of autophagy in
602 mammalian cells. *Sci. Rep.* (2020) doi:10.1038/s41598-020-68607-w.
603 63. Hirschenberger, M. *et al.* Luciferase reporter assays to monitor interferon signaling
604 modulation by SARS-CoV-2 proteins. *STAR Protoc.* **2**, 100781 (2021).
605 64. Diemen, F. R. van *et al.* CRISPR/Cas9-Mediated Genome Editing of Herpesviruses Limits
606 Productive and Latent Infections. *PLOS Pathog.* **12**, e1005701 (2016).
607 65. Sanjana, N. E., Shalem, O. & Zhang, F. Improved vectors and genome-wide libraries for
608 CRISPR screening. *Nat. Methods* **11**, 783–784 (2014).
609 66. Bryant, J. D., Lei, Y., VanPortfliet, J. J., Winters, A. D. & West, A. P. Assessing
610 Mitochondrial DNA Release into the Cytosol and Subsequent Activation of Innate Immune-
611 related Pathways in Mammalian Cells. *Curr. Protoc.* **2**, e372 (2022).
612 67. Radamaker, L. *et al.* Role of mutations and post-translational modifications in systemic AL
613 amyloidosis studied by cryo-EM. *Nat. Commun.* **12**, 6434 (2021).
614 68. MaxQuant enables high peptide identification rates, individualized p.p.b.-range mass
615 accuracies and proteome-wide protein quantification - PubMed.
616 https://pubmed.ncbi.nlm.nih.gov/19029910/.

69. Cox, J. *et al.* Andromeda: a peptide search engine integrated into the MaxQuant environment. *J. Proteome Res.* **10**, 1794–1805 (2011).

70. Mi, H. *et al.* PANTHER version 16: a revised family classification, tree-based classification tool, enhancer regions and extensive API. *Nucleic Acids Res.* **49**, D394–D403 (2021).

71. Mi, H. *et al.* Protocol Update for Large-scale genome and gene function analysis with PANTHER Classification System (v.14.0). *Nat. Protoc.* **14**, 703–721 (2019).

72. Costes, S. V. *et al.* Automatic and Quantitative Measurement of Protein-Protein Colocalization in Live Cells. *Biophys. J.* **86**, 3993–4003 (2004).

73. Valente, A. J., Maddalena, L. A., Robb, E. L., Moradi, F. & Stuart, J. A. A simple ImageJ macro tool for analyzing mitochondrial network morphology in mammalian cell culture. *Acta Histochem.* **119**, 315–326 (2017).

74. Osseforth, C., Moffitt, J. R., Schermelleh, L. & Michaelis, J. Simultaneous dual-color 3D STED microscopy. *Opt. Express* **22**, 7028–7039 (2014).

75. Read, C., Schauflinger, M., Nikolaenko, D., Walther, P. & von Einem, J. Regulation of Human Cytomegalovirus Secondary Envelopment by a C-Terminal Tetralysine Motif in pUL71. *J. Virol.* **93**, e02244-18 (2019).

76. Walther, P. & Ziegler, A. Freeze substitution of high-pressure frozen samples: the visibility of biological membranes is improved when the substitution medium contains water. *J. Microsc.* **208**, 3–10 (2002).

77. Wieland, J. *et al.* Zika virus replication in glioblastoma cells: electron microscopic tomography shows 3D arrangement of endoplasmic reticulum, replication organelles, and viral ribonucleoproteins. *Histochem. Cell Biol.* **156**, 527–538 (2021).

78. Kremer, J. R., Mastronarde, D. N. & McIntosh, J. R. Computer Visualization of Three-Dimensional Image Data Using IMOD. *J. Struct. Biol.* **116**, 71–76 (1996).

79. Weibel, E. R. Stereological Principles for Morphometry in Electron Microscopic Cytology11The personal work of the author was supported by Grant No. 3952 from the Schweizerischer Nationalfonds zur Förderung der Wissenschaftlichen Forschung, and by Grant No. 78 from BIGA. in *International Review of Cytology* (eds. Bourne, G. H., Danielli, J. F. & Jeon, K. W.) vol. 26 235–302 (Academic Press, 1969).

80. Sun, W., Vanhooke, J. L., Sondek, J. & Zhang, Q. High-throughput fluorescence polarization assay for the enzymatic activity of GTPase-activating protein of ADP-ribosylation factor (ARFGAP). *J. Biomol. Screen.* **16**, 717–723 (2011).

81. Ashkenazy, H. *et al.* ConSurf 2016: an improved methodology to estimate and visualize evolutionary conservation in macromolecules. *Nucleic Acids Res.* **44**, W344–W350 (2016).

FIGURE LEGENDS

Figure 1. Genetic Identification of ARF1 R99C and clinical phenotype. a-g, Erythematous vasculitic chilblain-like lesions on the hands (**a**) and face (**b**) of Patient 1. Right hand of the same patient showing frank tissue loss (**c**). Similar lesions were observed on the hands and feet of patients (**d**, **e, f**, **g**). **h**, Schematic overview of the domain structure of ARF1. Residue R99 is indicated by a red arrow. SW, Switch domain. **i**, Multiple sequence alignment showing the conservation of residue R99 of ARF1 in indicated species. **j**, ISG profile of patient Patient 2 (red) compared to the average of 29 healthy donors (blue).

Figure 2. Expression of ARF1 R99C induces a STING dependent type I IFN response. a, SEAP reporter gene assays to assess the impact of transient expression of FLAG-tagged ARF1

WT, R99C, Q71L or T31N on ISRE promoter induction in 293-Dual-hSTING-R232 reporter cells. SEAP expression was quantified 32 hours (h) post transfection and normalised to cell viability. Dots represent mean of n = 3 ± SEM (biological replicates). Lower panel: Corresponding immunoblots of whole cell lysates (WCLs) showing the corresponding expression of ARF1 WT R99C, Q71L and T31N stained with anti-FLAG. **b**, Area under the curve analysis of the data in (**a**). **c**, Impact of FLAG-tagged ARF1 WT and R99C expression by transient transfection on ISRE promoter activity in HEK293T cells co-expressing STING (+STING) or empty vector (-STING). ISRE-driven Firefly luciferase (Fluc) was quantified 32 h post transfection and normalised to GAPDH-promoter driven Renilla luciferase. Dots represent mean of n = 3 ± SEM (biological replicates). Lower panel: Corresponding immunoblots of WCLs showing the expression of ARF1 mutants, stained by anti-FLAG. **d**, Impact of ARF1 WT and R99C delivered by lentiviral transduction on ISRE promoter activity in A549 Dual reporter cells. IFN-β (1000 U/mL, 16 h) and cGAMP (10 µg/ml, 16 h) served as positive controls. Bars represent mean of n = 3 ± SEM (biological replicates). Lower panel: Corresponding immunoblots of WCLs stained by anti-FLAG, anti-STING and anti-GAPDH. **e**, Impact of ARF1 WT and R99C delivered by lentiviral transduction on NF-κB promoter activity in A549 Dual reporter cells quantified via SEAP activity. IFN-β (1000 U/mL, 16 h) and cGAMP (10 µg/ml, 16 h) served as positive controls. Bars represent mean of n = 3 ± SEM (biological replicates). Lower panel: Corresponding immunoblots of WCLs stained by anti-FLAG, anti-STING and anti-GAPDH. **f**, Exemplary immunoblot of WCLs of HEK293T cells transiently expressing vector or indicated ARF1 mutants as well as cGAS and STING. Blots were stained with anti-pTBK1, anti-TBK1, anti-IRF3, anti-FLAG and anti-GAPDH. **g**, Quantification of the band intensities in (**f**) for pTBK1 normalized to the band intensities of TBK1, in the presence of cGAS/STING. Bars represent mean of n = 3 ± SEM (biological replicates). **h**, Impact of ARF1 WT and R99C expression on ISG induction in primary normal

human lung fibroblasts (NHLF) as assessed by qPCR of OAS1 mRNA 72 h post transduction. IFN-β (1000 U/mL, 16 h) and cGAMP (10 µg/ml, 16 h) served as positive controls. Bars represent mean of n = 3-6 ± SEM (biological replicates). Lower panel: Corresponding immunoblots of WCLs stained by anti-FLAG, anti-STING and anti-GAPDH. **i**, Impact of supernatant (SN) from primary fibroblasts from healthy donors (n1, f1) or a patient (Patient 1) on ISRE promoter activity in 293-Dual-hSTING-R232 cells. IFN-β (100 U/mL, 48 h) and cGAMP (10 µg/ml, 48 h) served as positive controls. SEAP activity was quantified 48 h post SN transfer and normalised to cell viability. Bars represent mean of n = 3 ± SEM (biological replicates).

Figure 3: ARF1 R99C disrupts mitochondria, releasing mtDNA into the cytoplasm. a, Induction of the ISRE promoter in THP-1-Dual WT (grey) and THP-1-Dual KO-cGAS (pink) cells transduced with lentiviral vectors expressing ARF1 WT or R99C as indicated, quantified by Lucia luciferase (LLuc) activity 72 h post transduction. IFN-β (1000 U/mL, 16 h) and cGAMP (10 µg/ml, 16 h) served as positive controls. Bars represent mean of n=3 ± SEM (biological replicates). Lower panel: Corresponding immunoblots of WCLs stained by anti-FLAG, anti-STING, anti-cGAS and anti-GAPDH. **b**, Exemplary electron microscopy analysis of HEK293T cells transiently transfected with ARF1 WT or ARF1 R99C as indicated. Mitochondria (m) are highlighted in insets in bottom panels. Electron-dense granules and inflated cristae are highlighted by black and white arrows, respectively. Annotations: cp, cytoplasm; er, endoplasmic reticulum; g, Golgi apparatus; lv, large vesicle; ly, lysosome; m, mitochondria; nc, nucleus. **c,** Exemplary immunoblots showing fractionation of ARF1 WT, R99C, Q71L and vector transfected HEK293T cells as indicated. WCLs and fraction blots stained by anti-FLAG, anti-TFAM (mitochondria), anti-LAMIN B1 (nucleus) and anti-GAPDH (cytosol). **d**, qPCR of mtDNA (MT-D-Loop) in the cytosolic fraction of (**c**) relative to total normalized cellular mtDNA (mtDNA/nuclear DNA) using the ΔΔCT

712 method. n = 3 ± SEM. **e**, qPCR of mtDNA (MT-D-Loop) in the cytosolic fraction of primary
713 fibroblasts from healthy donors (n2, f1, I7) or a patient (Patient 1) relative to total normalized
714 cellular mtDNA (mtDNA/nuclear DNA) using the ΔΔCT method. n = 5 ± SEM. **f**, qPCR of
715 representative ISG *OAS1* in U2OS cells stably expressing STING and depleted of mtDNA by ddC,
716 or untreated (NT), upon transfection with empty vector, ARF1 WT or R99C n=3 ± SEM. **g**,
717 Exemplary immunoblot of WCLs of HEK293T cells transiently expressing ARF1 WT, R99C or
718 vector. Blots were stained with anti-MFN1, anti-RHOT1, anti-FLAG and anti-GAPDH.
719 Quantification of the band intensities for MFN1 normalized to the band intensities of GAPDH.
720 Bars represent mean of n = 6 ± SEM (biological replicates). **h,** Exemplary immunoblots showing
721 fractionation of HEK293T cells expressing ARF1 WT, R99C or vector control as well as VCP.
722 WCLs and fraction blots stained by anti-FLAG, anti-HA, anti-TFAM (mitochondria), anti-
723 LAMIN B1 (nucleus) and anti-GAPDH (cytosol). **i**, qPCR of mtDNA (MT-D-Loop) in the
724 cytosolic fraction of (**h**) relative to total normalized cellular mtDNA (mtDNA/nuclear DNA) using
725 the ΔΔCT method. n = 5 ± SEM.

726

727 **Figure 4. GTPase activity of ARF1 R99C is reduced. a**, Model of ARF1 (PDB: 2J59) in ATP-
728 bound form. R99 and D26 are highlighted. Phosphates in orange. **b**, Interaction of ARF1 WT with
729 GTP analysed by fluorescence thermal shift assay. **c**, Protein stability of ARF1 R99C and its
730 interaction with GTP analysed by fluorescence thermal shift assay. Data are representative of two
731 biological replicates. **d**, GTPase activity quantified by GTPase Glo assay of indicated ARF1
732 mutants purified from HEK293T cells expressing FLAG-ARF1 WT and mutants. Lower panel:
733 Corresponding immunoblot (one representative) stained with anti-FLAG displaying input
734 amounts. Bars represent mean of n = 4 ± SEM (biological replicates). **e**, Impact of expression of
735 ARF1 WT and R99C co-expressed with indicated GEF or GAP on ISRE promoter activity in 293-

Dual-hSTING-R232 reporter cells quantified by SEAP activity normalized to cell viability. Corresponding immunoblots of WCLs were stained with anti-HA, anti-turboGFP (tGFP), anti-FLAG, anti-STING and anti-GAPDH. Bars represent mean of n = 3 ± SEM (biological replicates). **f**, Fold changes (log 10) of protein abundance in ARF1 WT versus R99C large scale purification from HEK293T cells. Co-purifying proteins were assessed by SILAC mass spectrometry. Components of the COPI machinery are highlighted in pink and annotated. **g**, Gene Ontology Analysis (PantherDB) of the top 100 downregulated genes as determined in (**f**). Fold enrichment of individual GO terms versus the -log P value is shown. FACT complex (GO:0035101), MCM complex (GO:0042555), CMG complex (GO:0071162), COPI vesicle coat (GO:0030126), DNA replication preinitiation complex (GO:0031261), chaperonin-containing T-complex (GO:0005832), eukaryotic translation initiation factor 3 complex, eIF3m (GO:0071541), COPI-coated vesicle membrane (GO:0030663), methylosome (GO:0034709), COPI-coated vesicle (GO:0030137). Colour highlights the top 10 GO terms; orange, non-COPI terms; pink, COPI-related GO terms.

Figure 5: ARF1 is responsible for retrograde transport from the Golgi/ERGIC to the ER. **a**, Impact of FLAG-tagged ARF1 WT or R99C expression by transient transfection on ISRE promoter activity in 293-Dual-hSTING-R232 cells either mock treated or treated with cGAMP (1.25 µg/ml, 5 µg/ml; 16 h). SEAP activity was quantified 32 h post transfection and normalized to cell viability. Bars represent mean of n = 3 ± SEM (biological replicates). Lower panel: representative corresponding immunoblot stained with anti-FLAG, anti-STING and anti-GAPDH. **b**, Area under the curve analysis of the data in (**a**). **c**, Type I IFN signalling activation by expression of ARF1 WT and R99C in the presence of indicated STING mutants in HEK93T cells, assessed by ISRE-promoter firefly luciferase reporter gene assay 32 h post transfection, normalised to

GAPDH-promoter driven Renilla luciferase. Bars represent mean of n = 3 ± SEM (biological replicates). **d**, Representative electron microscopic images of HEK293T cells expressing the indicated ARF1 mutants. Exemplary electron microscopic images with (bottom) and without (top) highlighted luminal area are shown. Scale bar, 0.5 µm **e**, Golgi/ERGIC luminal volume and **f**, associated vesicle volume quantified in tomograms of cells in (**d**), as assessed as percentage of the total volume of the analysed section. Bars represent mean of n = 9 ± SEM (images). **g**, Quantification of particles of ERGIC-53 staining (left panel), particle size (middle panel) or the total are (right panel), in HeLa cells transiently expressing ARF1 WT, R99C, Q71L or T31N. Cells were stained 24 h post transfection with anti-ERGIC-53 and anti-FLAG. Black lines represent mean of n = 39-61 ± SEM (individual cells). **h**, Pearson's correlation coefficient indicating the co-localisation between GM130 and thermosensitive VSV-G (VSVG-ts045) in HeLa cells transfected with VSVG-ts045-KDELR and vector control, ARF1 WT or ARF1 R99C. Cells were incubated at 37 °C for 24 h, then either fixed or further incubated at 32 °C for 2 h and then either fixed or shifted to 40 °C for 1 h and fixed. Temperature shifts (37 °C/32 °C/40 °C) as indicated. Lines represent mean of n = 14-29 ± SEM (cells).

Figure 6: STING accumulates at the ERGIC in the presence of ARF1 R99C. a, Exemplary **c**onfocal laser scanning microscopy images of STING-eGFP (green) and indicated FLAG-tagged ARF1 mutants in HeLa cells. Details are shown as higher magnification insets. Cells were stained 24 h post transfection with anti-FLAG (red) and anti-GM130 (grey). Nuclei, DAPI (blue). Scale bar, 10 µm. **b**, Quantification of the co-localisation of ARF1 and GM130 and **c**, STING and GM130 from the images shown in (**a**), using Pearson's correlation coefficient. Lines represent mean of n = 19-26 ± SEM (individual cells). **d**, Exemplary **c**onfocal laser scanning microscopy images and respective high-magnification insets of primary fibroblasts from a healthy donor or

patient 1. The cells were either mock treated or treated with cGAMP (10 µg/ml, 3 h) and stained with anti-STING (green) and anti-GM130 (grey). Nuclei, DAPI (blue). Scale bar, 10 µm. **e**, Quantification of the co-localisation of STING and GM130 from the images shown in (**d**), using Pearson's correlation coefficient. Lines represent mean of n = 60-65 ± SEM (individual cells). **f**, Exemplary STED super-resolution microscopy images and respective high-magnification insets of NHLF cells transduced with lentiviruses expressing indicated ARF1 constructs or empty vector. 48 h post transduction the cells were stained with anti-STING (green), anti-FLAG (not shown) and anti-GM130 (red). Only FLAG-staining positive cells are displayed. Scale bar, 10 µm. **g**, Presence and localisation of pTBK1 (green) in relation to ARF1 (FLAG; red) and ERGIC53 (white) in NHLF cells transduced with lentiviruses expressing indicated ARF1 constructs or empty vector. Details are shown as higher magnification insets. cGAMP (10 µg/ml, 3 h) was used as positive control. Scale bar, 5 µm. **h**, Quantification of the area (in pixels) of pTBK1 puncta observed in (**g**). Lines represent mean of n = 57-96 ± SEM (individual cells).

MATERIALS AND METHODS

Cell culture. HEK293T (ATCC), HEK293T ATG5 KO, Hela (ATCC), 293-Dual-hSTING-R232 (Invivogen), A549-Dual (Invivogen) cell lines, normal human lung fibroblast primary cells (Lonza) and normal human dermal fibroblasts primary cells (Thermo Fisher, Innoprot and Promocell) were cultivated in Dulbecco's Modified Eagle Medium (DMEM) supplemented with 10% (v/v) fetal bovine serum (FBS), 100 U/ml penicillin, 100 µg/ml streptomycin, and 2 mM L-glutamine. THP-1-Dual and THP-1-Dual KO-cGAS (both Invivogen) cells were cultivated in RPMI 1640 medium supplemented with 10% (v/v) fetal bovine serum (FBS), 100 U/ml penicillin, 100 µg/ml streptomycin, and 2 mM L-glutamine. U2OS cells (ATCC) were maintained in McCoy

807 medium (Invitrogen) supplemented with 10% (v/v) fetal bovine serum. All cells were incubated at
808 37°C in a 5% CO_2, 90% humidity atmosphere. Patient cells are from Patient 1 were isolated by
809 skin punch biopsy and cultivated as the other dermal fibroblast cells.
810 **Ethics**. Clinical information and samples were obtained with informed consent. The study
811 was approved by the Comité de Protection des Personnes (ID-RCB/EUDRACT: 2014-A01017-
812 40) in France, and the Leeds (East) Research Ethics Committee (REC reference:
813 10/H1307/2 IRAS project ID: 62971) in the UK. ARF1 patient cells were handled with approval
814 of the Ethics Committee at Ulm University (Approval 530/21).
815 **Expression constructs and cloning.** A construct coding for human ARF1 (pCMV6-hARF1-myc-
816 FLAG) was purchased from Origene (kindly provided by Michaela Gack, Florida). Mutations in
817 R99C, Q71L and T31N were introduced by Q5 site-specific mutagenesis (see primers in table 1).
818 Constructs coding for cGAS 3×-FLAG and STING-FLAG were kindly provided by Jae U. Jung
819 (University of Southern California). STING-FLAG mutations R238A/Y240A and S366A were
820 introduced by Q5 site-specific mutagenesis (see primers in table 1). pEGFP-VSVG was a gift from
821 Jennifer Lippincott-Schwartz (Addgene plasmid # 11912[60]). ECFP-ELP1-25 was a gift from
822 Michael Davidson (Addgene plasmid # 55341). The open reading frame (ORF) of KDELR (ELP1)
823 was subcloned into the pEGFP-VSVG vector using Gibson assembly (New England Biolabs). The
824 insert was amplified by PCR (see primers in table 1) and the vector linearized with EcoRI and
825 ApaI restriction enzymes (New England Biolabs). The ORF of TagRFP (from pCR3-TagRFP) was
826 subcloned into the pCMV6-hARF1-myc-FLAG vector and the pCMV6-hARF1-R99C-myc-
827 FLAG vector using Gibson assembly. The insert was amplified by PCR (see primers in table 1)
828 and the vectors were linearized with MluI and PmeI restriction enzymes (New England Biolabs).
829 To insert the ORFs of ARF1 WT or ARF1 R99C (from pCMV6-ARF1, Origene) in a lentiviral
830 backbone, both ORFs together with IRES-Puro (from pIRES-TRIM2-FLAG) were subcloned into

the pBoB-hCas9-IRES-Bla vector using Gibson assembly. The inserts were amplified by PCR (see primers in table 1) and the vector was linearized with XbaI and PmeI restriction enzymes (New England Biolabs). Constructs coding for human ARFGAP1 (pCMV3-ARFGAP1-HA)) and VCP (pCMV3-VCP-HA) were purchased from Sino Biologicals. pGAPDH_PROM_01_Renilla SP Luciferase and pISRE-FLuc plasmids were described previously[61]. Human STING ORF was amplified from pMSCV-hygro-STING plasmid (Addgene #102598) by PCR (see primers in table 1) and inserted into linearized pEGFP-C3 (Clontech) using XhoI and EcoRI enzymes (New England Biolabs). pCMV6-ARFGEF1-TurboGFP was purchased from Clinisciences (RG222817).

Table 1: Primers used for cloning.

Name	Sequence 5' – 3'
ARF1-Q71Lfwd	TTG GAC AAG ATC CGG CCC CTG TGG
ARF1-Q71Lrev	GCC ACC CAC GTC CCA CAC AGT
ARF1-T31N-fwd	AAT ACG ATC CTC TAC AAG CTT AAG CTG GGT GAG A
ARF1-T31N-rev	CTT CCC TGC AGC ATC CAG GCC
ARF1 R99Cfwd	GAG TGT GTG AAC GAG GCC CGT GAG GAG C
ARF1 R99Crev	TCT GTC ATT GCT GTC CAC CAC GAA GAT C
STING-R238A/Y240A-fwd	CAT CAA GGA TGC GGT TGC CAG CAA CAG CAT C
STING-R238A/Y240A-rev	CCA GCA CGG TCA GCG GTC TG
STING-S366A-fwd	GCT CCT CAT CGC TGG AAT GGA AAA GCC C

STING-S366A-rev	TCA GGC TCT TGG GAC ATC
VSVG(tsO45)-KDELR-fwd	GAC TTG GAA ACA GAA TTC TGA TGG CCA TGA ACA TTT TCC G
VSVG(tsO45)-KDELR-rev	CTC ACC ATT GGA TCC CGG GCC CCT GCT GGC AAA CTG AGC TTC T
ARF1-TagRFP-fwd	GTC CAA TCA GCT CCG GAA CCA GAA GGC GGT GTC TAA GGG CGA AG
ARF1-TaqRFP-rev	CAG CTA TGA CCG CGG CCG GCC GT T TTT AAT TAA GTT TGT GCC CC
pBOB-ARF1-fwd	CCT CCA TAG AAG ACA CCG ACT CTA GAG CCA CCA TGG GGA ACA TCT TCG CC
pBOB-ARF1-rev	CTA TGA CCG CGG CCG GCC GTT TAA ACC TTA TCG TCG TCA TCC
pBOB-IRES-Puro-fwd	ACG GCC GGC CGC GGT CAT AGG CGG CCG CTC TAG CCC AAT TCC
pBOB-IRES-Puro-rev	GCT CCA TGT TTT TCC AGG TTT TCA GGC ACC GGG CTT GCG
EGFP-STING-fwd	ATT ACT CGA GAT GCC CCA CTC CAG
EGFP-STING-rev	GAA TTC TCA AGA GAA ATC CGT GCG GA

841

842 **Transfection of mammalian cells.** DNA of expression vectors was transiently transfected using
843 either the TransIT-LT1 Transfection Reagent (Mirus) or Polyethylenimine (PEI, 1 mg/ml in H2O)
844 according to the manufacturers recommendations or as described previously [62].

Transduction of mammalian cells. pMDLg, RSV-Rev, and pMD.G together with the generated pBOB constructs were used to rescue 3rd generation lentiviruses as previously described[61,62]. Cells were incubated with 3rd generation lentiviral particles for 16 h. Subsequently, the cells were washed three times with DMEM and incubated for further 48 h.

Whole-cell lysates. Whole-cell lysates were prepared by harvesting cells in Phosphate-Buffered Saline (PBS, Gibco). If not mentioned otherwise, the cell pellet (500 g, 4 °C, 5 min) was lysed as previously described[62] in transmembrane lysis buffer (150 mM NaCl, 50 mM 4-(2-hydroxyethyl)-1-piperazineethanesulfonic acid (HEPES) pH 7.4, 1% Triton X-100, 5 mM ethylenediaminetetraacetic acid (EDTA)) by vortexing at maximum speed for 30 s. Cell debris was removed by centrifugation (20,000 g, 4 °C, 20 min), and the protein concentration of the supernatants was quantified using a BCA assay (Pierce Rapid Gold BCA Protein Assay Kit, Thermo Fisher Scientific). The lysates were then stored until analysis at -20 °C.

SDS-PAGE and Immunoblotting. SDS-PAGE and immunoblotting was performed using standard techniques as previously described[62]. In brief, whole cell lysates were mixed with 6x Protein Sample Loading Buffer (LI-COR, at a final dilution of 1x) supplemented with 15% β-mercaptoethanol, heated to 95°C for 5 min, separated on NuPAGE 4-12% Bis-Tris Gels (Invitrogen) for 90 minutes at 90 V and blotted onto Immobilon-FL PVDF membranes (Merck Millipore). The transfer was performed at a constant voltage of 30 V for 30 min. After the transfer, the membrane was blocked in 1% Casein in PBS. Proteins were stained with primary antibodies mouse anti-FLAG M2 (1:5000, Sigma-Aldrich), sheep anti-STING (1:1000, Bio-Techne), rabbit anti-pTBK1 (1:1000, Cell Signaling), rabbit anti-TBK1 (1:1000, Cell Signaling), rabbit anti-IRF3 (1:1000, Cell Signaling), rabbit anti-HA (1:1000, Cell Signaling), rabbit anti-ARF1 (1:300, Proteintech), rabbit anti-cGAS (1:2000, Proteintech), rabbit anti-RFP (1:1000, Abcam), mouse anti-turboGFP (1:1000, Origene), rabbit anti-TFAM (1:1000, Proteintech), mouse anti-Lamin B1

(1:10,000, Proteintech), rat anti-GAPDH (1:1000, BioLegend), rabbit anti-MFN1 (1:1000, Cell Signaling), mouse anti-RHOT1 (1:1000, Abnova), mouse anti-Drp1 (1:1000, Cell Signaling), rabbit anti-pDrp1 (1:1000, Cell Signaling), rabbit anti-SURF4 (1.1000, Novus Biologicals) and subsequently Infrared Dye labelled secondary antibodies (LI-COR), diluted in 0.05% Casein in PBS. Band intensities were quantified using Image Studio lite (LI-COR).

Luciferase reporter assays. Luciferase reporter assays were performed as previously described in detail[63]. In brief, HEK293T cells were either transiently transfected with luciferase reporter constructs, or reporter cell lines (A549-Dual, 293-Dual hSTING-R232, THP-1-Dual or THP1-Dual KO-cGAS) were used. 32 h post- transfection or 72 h post transduction, cells were lysed in passive lysis buffer (Promega) and luciferase activities of the firefly luciferase (FFLuc), renilla luciferase, lucia luciferase or SEAP activity were determined. For HEK293T cells ISRE-firefly luciferase activities normalised to renilla activity were measured via DualGlo Luciferase Assay System (Promega). For the reporter cell lines ISRE-lucia luciferase activity (IFNb-lucia luciferase for 293-Dual hSTING-R232 cells) was measured 1 s after injecting 20 mM coelenterazine (PFK Biotech) and NF-κB-SEAP activity (ISRE-SEAP for 293-Dual hSTING-R232 cells) via Alkaline Phosphatase Blue Microwell Substrate (Sigma-Aldrich). Both were normalized to cell viability determined by the CellTiter-Glo Luminescent Cell Viability Assay (Promega). Luciferase and cell viability measurements were performed using an Orion II microplate Luminometer (Berthold), SEAP activity was measured at 650 nm by using a Vmax kinetic microplate reader (Molecular Devices) and the SoftMax Pro 7.0.3 software.

Generation of U2OS cells stably expressing STING and mtDNA depletion. The pMSCV-hygro plasmid carrying WT STING1 cDNA (Addgene plasmid #102598) or empty vector were used in combination with packaging vector pCL-Ampho (Novus) and envelope vector pCMV-VSV-G (Addgene plasmid #8454) to produce retroviral vectors as described for lentiviral vectors. 100,000

U2OS cells were transduced with 0.5 mL retroviral vectors, 8 µg/mL polybrene (Millipore) and 10 mM HEPES (Invitrogen) in 12-well plates, and medium replaced 24 hours later. Two days after transduction, transduced cells were selected and maintained in culture with 200 µg/mL hygromycin B (Invivogen). STING expression was verified by western blotting. mtDNA depletion in U2OS and U2OS-STING cells was induced by 100 µM 2',3' dideoxycytidine (ddC, Sigma-Aldrich) treatment in medium supplemented with 50 µg/mL uridine (Sigma-Aldrich) and 1 mM sodium pyruvate (GIBCO) for seven to fourteen days before use. To control for mtDNA depletion, total DNA from 500,000 cells was extracted using the DNeasy Blood and Tissue Kit (Qiagen), following the manufacturer's instructions. DNA concentrations were determined by photometry (Nanodrop) and 15 ng and 7.5 ng DNA were used to perform qPCR for the mitochondrial gene MT-COXII and the nuclear gene GAPDH (see primers in Table 3). Quantitative PCR (qPCR) was performed using Power SYBR Green (Invitrogen). Ratios of ΔΔCt for MT-COXII over GAPDH for the different DNA concentrations were averaged and the fold change to untreated (UT) is shown in figures. U2OS cells were stimulated for 4 hours with 2 µg/mL HT-DNA (Sigma-Aldrich) complexed with Lipofectamine 2000 (Invitrogen), according to the manufacturer's instructions, or lipofectamine alone.

Generation of HEK293T ATG5 KO cells. HEK293T ATG5 KO cells were generated by genomic knock out using CRISPR Cas9. To this end, 3rd generation lentiviral vectors were generated as described before[62] using pSicoR-CRISPR-PuroR CRISPR/Cas9[64] constructs harboring an ATG5 targeting sgRNA or a non-targeting (NT) sgRNA. (NT: ACGGAGGCTAAGCGTCGCAA, ATG5: AACTTGTTTCACGCTATATC)[65] as the transfer plasmid. HEK293T cells were transduced with the lentiviral vectors and 3 days post-transduction separated into individual cells using limited dilution. The individual cells were grown into clonal cell lines and screened for ATG5 KO using Western blot analysis (anti-ATG5 antibody, Cell

Signaling Technology, #2630). Clones with a conformed knock out were expanded and stocks were conserved by cryo preservation.

Overexpression of WT and mutant ARF1 in U2OS cells. U2OS WT and U2OS-STING cells plated in 12-well plates were transiently transfected with ARF1 WT, ARF1 R99C or empty vector. Cells were collected 24 hours later for RNA and protein analysis. Total RNA was extracted using the RNAqueous-Micro Kit (Ambion), and reverse transcription performed with the High-Capacity cDNA Reverse Transcription Kit (Applied Biosystems). Levels of cDNA were quantified by RT-qPCR using TaqMan Gene Expression Assay (Applied Biosystems). Differences in cDNA inputs were corrected by normalization to HPRT1 cDNA levels. Relative quantitation of target cDNA was determined by the formula 2-ΔΔCT (See Taqman probes in table 4). For whole cell lysate analysis, proteins were extracted from U2OS cells using RIPA lysis buffer with 1% protease inhibitor and 1% phosphatase inhibitor. Bolt LDS Sample Buffer (4X, Novex Life Technologies) and Bolt Sample Reducing agent (10X, Novex Life Technologies) were added to protein lysates, samples resolved on 4-12 % Bis-Tris Plus NuPAGE gels (Invitrogen) and then transferred to nitrocellulose membrane for 7 min at 20 V using the iBlot 2 Dry Blotting System (Invitrogen). To analyse protein phosphorylation status, membranes were blocked in LI-COR buffer, and primary phospho-antibodies (rabbit anti-pIRF3, 1:1000; rabbit anti-pSTING, 1:1000, Cell Signaling) incubated for 48 hours in blocking solution. For cofilin immunoblot, membranes were blocked with 5% non-fat milk in TBS, and primary antibodies (rabbit anti-Cofilin, 1:1000, Cell Signaling) incubated overnight at 4°C in 1.5% Bovine Serum Albumin in TBS buffer supplemented with 0.1% Tween. After stripping, membranes were reblotted with anti-STING antibodies (mouse anti-STING, 1:1000, R&D Systems; rabbit anti-IRF3, 1:1000, Cell Signalling) in 2.5% non-fat milk in TBS buffer supplemented with 0.1% Tween. After washing, membranes were incubated with appropriate anti-mouse or anti-rabbit secondary antibodies for 45 minutes at room temperature

(LI-COR). Signal was detected using the OdysseyCLx System (LI-COR). Comparative signal analyses were performed using Fiji (ImageJ).

Assessing mitochondrial DNA release into the cytosol. HEK293T WT or HEK293T ATG5 KO cells were transfected with ARF1 WT, ARF1 R99C or empty vector. Alternatively, HEK293T WT cells were transfected with ARF1 WT, ARF1 R99C or empty together with VCP or empty vector. 24 h later, cells were treated with 10 µM of ABT-737 and 10 µM Quinoline-Val-Asp-Difluorophenoxymethylketone (Q-VD-OPH) as a positive control. In the case of primary human dermal fibroblasts, cells from four healthy donors or from patient 1 were used. On the next day, the cells were harvested and isolation and quantification of DNA from cytosolic, mitochondrial and nuclear fractions was performed as described previously[66] (basic protocol 2). Briefly, half of the cells were lysed in SDS lysis buffer (20 mM Tris, pH 8, 1% (v/v) SDS, protease inhibitors) to obtain WCLs for normalisation, whereas the other half was used for fractionation. Cytosolic, mitochondrial and nuclear extracts were isolated by subsequently incubating the cells with saponin lysis buffer (1x PBS, pH 7.4, 0.05% saponin , protease inhibitors), NP-40 lysis buffer (50 mM Tris, pH 7.5, 150 mM NaCl, 1 mM EDTA, 1% (v/v) NP-40, 10% (v/v) glycerol, protease inhibitors) and SDS lysis buffer (20 mM Tris, pH 8, 1% (v/v) SDS, protease inhibitors), respectively. Purity of the fractions was determined by immunoblotting for GAPDH (cytosolic extract), TFAM (mitochondrial extract), and Lamin B1 (nuclear extract). DNA extraction of the fractions and WCLs was performed using phenol-chloroform. DNA concentrations were determined by photometry (Nanodrop) and equal amounts of DNA were used to perform qPCR for mitochondrial DNA (MT-Dloop) and nuclear DNA (KCNJ10) (see primers in Table 3). qPCR was performed using PowerUP SYBR Green (Applied Biosystems) and the relative cytosolic mtDNA was calculated using the ΔΔCT method.

Table 3: Primers used for SYBR Green qPCR.

Type	Primers	Sequence
SYBR Green	MT-COXII_F	CGTCTGAACTATCCTGCCCG
SYBR Green	MT-COXII_R	TGGTAAGGGAGGGATCGTTG
SYBR Green	GAPDH_F	ATGCTGCATTCGCCCTCTTA
SYBR Green	GAPDH_R	GCGCCCAATACGACCAAATC
SYBR Green	KCNJ10 fwd	GCGCAAAAGCCTCCTCATT
SYBR Green	KCNJ10 rev	CCTTCCTTGGTTTGGTGGG
SYBR Green	MT-Dloop fwd	CATAAAGCCTAAATAGCCCACACG
SYBR Green	MT-Dloop rev	CCGTGAGTGGTTAATAGGGTGATA

Expression of WT and mutant ARF1 in NHLF cells. NHLF cells were transduced with lentiviral particles coding for ARF1 WT, ARF1 R99C or empty vector. For qPCR analysis, total RNA was extracted 72 h post transduction using the Quick-RNA Microprep Kit (Zymo research) according to the manufacturer's instructions. Reverse transcription and qRT–PCR were performed in one step using the SuperScript III Platinum Kit (Thermo Fisher Scientific) on a StepOnePlus Real-Time PCR System (Applied Biosystems) according to the manufacturer's instructions. TaqMan probes for each individual gene were acquired as premixed TaqMan Gene Expression Assays (Thermo Fisher Scientific) and added to the reaction (See probes in table 4). Expression levels for each target gene were calculated, e.g. for OAS1 expression levels by normalizing to GAPDH cDNA levels using the ΔΔCT method.

Table 4: Primers used for TaqMan qPCR.

Type	Primers	Assay ID
TaqMan	HPRT1	Hs03929096_g1

TaqMan	IFI27	Hs01086370_m1
TaqMan	RSAD2	Hs01057264_m1
TaqMan	OAS1	Hs00973637_m1
TaqMan	MX1	Hs00895608_m1
TaqMan	IFNB1	Hs01077958_s1

978

979 **Dimerization assay.** HEK293T cells were transfected with ARF1 WT (pCMV6-ARF1-myc-
980 FLAG or pCMV6-ARF1-Tag-RFP, or with pCMV6-ARF1-myc-FLAG and pCMV6-ARF1-Tag-
981 RFP) or ARF1 R99C (pCMV6-ARF1-R99C-myc-FLAG or pCMV6-ARF1-R99C-Tag-RFP, or
982 with pCMV6-ARF1-R99C-myc-FLAG and pCMV6-ARF1-R99C-Tag-RFP). 24 h post
983 transfection, WCLs were prepared and input samples were saved for western blotting. The WCLs
984 were incubated with anti-FLAG M2 magnetic beads (Sigma-Aldrich) for 4 h at 4 °C on a rotating
985 shaker. Subsequently, the beads were washed five times with transmembrane lysis buffer and
986 incubated with 1x Protein Sample Loading Buffer supplemented with 15% β-mercaptoethanol.
987 After heating to 95°C for 10 min the samples were applied to SDS-PAGE and immunoblotting.

988 ***In vitro* GTPase assays.** HEK293T cells were transfected with pCMV6-ARF1-myc-FLAG,
989 pCMV6-ARF1-R99C-myc-FLAG, pCMV6-ARF1-Q71L-myc-FLAG or pCMV6-ARF1-T31N-
990 myc-FLAG. 24 h later, WCLs were prepared in GTPase lysis buffer (150 mM NaCl, 50 mM
991 HEPES pH 7.4, 1% Triton X-100, 5 mM $MgCl_2$, 5 mM EDTA) and incubated with anti-FLAG
992 M2 magnetic beads (Sigma-Aldrich) for 4 h at 4 °C on a rotating shaker. Subsequently, the beads
993 were washed three times with washing buffer I (500 mM NaCl, 50 mM HEPES pH 7.4, 1% Triton
994 X-100, 5 mM $MgCl_2$, 5 mM EDTA) and twice with washing buffer II (100 mM NaCl, 50 mM
995 HEPES pH 7.4, 1% Triton X-100, 5 mM $MgCl_2$, 5 mM EDTA). Next, the beads were incubated
996 with GTPase-Glo-GEF assay buffer (Promega) and the GTPase reaction was performed according

997 to the manufacturer's recommendations (GTPase-Glo assay, Promega). In short, the beads were
998 incubated with 2x GTP solution for 16 h followed by the addition of the GTPase-Glo reagent and
999 the detection reagent. The resulting luminescence was measured using an Orion II microplate
1000 Luminometer (Berthold).

1001 **Stable isotope labelling of amino acids in cell culture (SILAC).** To analyse interaction partners
1002 of ARF1 WT and ARF1 R99C, stable isotope labelling of amino acids in cell culture (SILAC)-
1003 based quantitative mass spectrometry (MS) was performed. HEK293T cells were cultivated in
1004 SILAC medium light (DMEM for SILAC supplemented with 10% (v/v) dialyzed FBS, 100 U/ml
1005 penicillin, 100 µg/ml streptomycin, 2 mM L-glutamine, 200 mg/ml proline, 84 mg/ml L-arginine,
1006 146 mg/ml L-lysin) or SILAC medium heavy (DMEM for SILAC supplemented with 10% (v/v)
1007 dialyzed FBS, 100 U/ml penicillin, 100 µg/ml streptomycin, 2 mM L-glutamine, 200 mg/ml
1008 proline, 87.2 mg/ml $^{13}C^{15}N$-labelled L-arginine, 152.8 mg/ml $^{13}C^{15}N$-labelled L-lysin) for five
1009 passages to completely incorporate the labelled amino acids. Afterwards, the cells were either
1010 transfected with ARF1 WT (heavy) or ARF1 R99C (light). 24 h later, WCLs were prepared from
1011 $1x10^7$ cells and incubated with anti-FLAG M2 magnetic beads (Sigma-Aldrich) for 4 h at 4 °C on
1012 a rotating shaker. Subsequently, the beads were washed five times with transmembrane lysis buffer
1013 and incubated with 1x Protein Sample Loading Buffer supplemented with 15% β-mercaptoethanol.
1014 After heating to 95°C for 10 min the samples were applied to SDS-PAGE and immunoblotting or
1015 MS.

1016 **Mass spectrometry (MS) and data analysis.** SILAC labelled samples were combined in a 1-to-
1017 1 manner and proteins were separated using standard 12.5% SDS-Page followed by colloidal
1018 Coomassie staining and subsequent sample preparation as described earlier[67]. Samples were
1019 measured using an LTQ Orbitrap Velos Pro system (Thermo Fisher Scientific) online coupled to
1020 an U3000 RSLCnano (Thermo Fisher Scientific) as described previously[67]. Database search was

performed using MaxQuant Ver. 1.6.3.4 (www.maxquant.org)[68]. For peptide identification and quantitation, MS/MS spectra were correlated with the UniProt human reference proteome set (www.uniprot.org, Version on March 16th 2021), supplemented with the ARF1 sequences, employing the build-in Andromeda search engine [69]. The respective SILAC modifications and carbamidomethylated cysteine were considered as a fixed modification along with oxidation (M), and acetylated protein N-termini as variable modifications. False discovery rates were set on both, peptide and protein level, to 0.01. Subsequent data analysis was performed employing MS Excel and Origin Pro 2017G. For outlier analysis significance B was calculate using Perseus (https://maxquant.org/perseus/) and proteins with log2 rations were considered as regulated.

Go-Term Analysis. The top 100 genes less associated with ARF1 R99C compared to ARF1 WT according to the SILAC experiment were submitted to PantherDB[70,71]. Analysis Type: PANTHER Overrepresentation Test (Released 20220202). GO Ontology database DOI: 10.5281/zenodo.6399963, Released 2022-03-22. Reference List:Homo sapiens (all genes in database).

Immunofluorescence. Cells were seeded on coverslips (VWR) in 24-well plates and treated as indicated. Next, the samples were washed with PBS and fixed in 4% paraformaldehyde solution (PFA) for 20 min at RT, permeabilized and blocked with PBS containing 0.5 % Triton X-100 and 5 % FCS for 1 h at RT. Afterwards, the cells were washed with PBS and incubated for 2 h at 4 °C with primary antibody (mouse anti-FLAG M2, 1:400, Sigma-Aldrich; rabbit anti-GM130, 1:400, Cell Signaling; rabbit anti-ERGIC-53, 1:400, Proteintech; sheep anti-TGN46, 1:400, Bio-Rad; rabbit anti-pTBK1, 1:100, Cell Signaling; mouse anti-STING, 1:100, Novus Biologicals, rabbit anti-STING, 1:200, Proteintech)) diluted in PBS with 1 % FCS. After washing with PBS/0.1 % Tween 20, the samples were incubated with the secondary antibody (donkey anti-mouse IgG (H+L) Alexa Fluor Plus 568, donkey anti-mouse IgG (H+L) Alexa Fluor Plus 488, donkey anti-

rabbit IgG (H+L) Alexa Fluor Plus 647, donkey anti-sheep IgG (H+L) Alexa Fluor Plus 647, 1:400, Thermo Fisher Scientific) or with primary antibody-secondary antibody conjugates (rabbit anti-ERGIC-53, 1.25 µg/ml, Proteintech; rabbit anti-GM130, 0.585 µg/ml, Cell Signaling; rabbit anti p-TBK1, 1.42 µg/ml, Cell Signaling; rabbit anti-STING, 3.5 µg/ml, Proteintech; mouse anti-FLAG M2 0.35 µg/ml, Sigma-Aldrich; conjugated to equal amounts (µg/ml) of Zenon Alexa Fluor 647 rabbit IgG labelling reagent, Zenon Alexa Fluor 568 rabbit IgG labelling reagent, Zenon Alexa Fluor 488 rabbit IgG labelling reagent or Zenon Pacific Blue mouse IgG_{2a} labelling reagent, Thermo Fisher Scientific) and 500 ng/ml DAPI for 2 h at 4 °C in the dark. Next, the samples were washed with PBS/0.1 % Tween 20 and water and the cover slips were mounted onto microscopy slides. Images were acquired using a Zeiss LSM 710 confocal laser scanning microscope with ZEN imaging software (Zeiss). Images were analysed with ImageJ (Fiji). The number of ERGIC-53 positive particles and the particle size was analysed using a custom ImageJ macro (Fiji). Co-localization was determined with the Huygens Professional 19.04 software. In short, Pearson coefficients were calculated with the "Huygens Colocalization Analyzer" using the Costes method[72] and applying individual thresholds.

Live cell imaging of mitochondria and Mitochondrial Network Analysis (MiNA). HeLa cells were seeded in 35 mm µ-Dishes (Ibidi) and transfected with TagRFP-labelled ARF1 WT, ARF1 R99C or vector control. 24 h later, all cells were treated with 1 µM Mitotracker and 1 µg/mL Hoechst 33342 for 30 min at 37°C. Sequentially the medium was removed and exchanged by fresh medium without phenol red. Images were then acquired using a Zeiss LSM 710 confocal laser scanning microscope with ZEN imaging software (Zeiss). Images analysis was performed with ImageJ (Fiji) using the the background subtractor tool (MOSAIC group) and the MiNA plugin (StuartLab). First, the background subtractor (length=20) was used, then the despeckle command and finally single cells were examined using the MiNA Analyse morphology plugin

(threshold=moments)[73]. The values obtained for the mitochondrial footprint (area/volume consumed by mitochondrial signal) were then used for visualization.

VSVG transport assay. Retrograde transport of VSVG-ts045-KDELR was performed as described previously[43]. In brief, HeLa cells were transfected with pEGFP-VSVG-ts045-KDELR and ARF1 WT, ARF1 R99C or empty vector. The cells were incubated at 37 °C for 24 h and then directly fixed or incubated at 32 °C for 2 h to accumulate the fusion protein at the Golgi complex. Cells were then either fixed or shifted to 40 °C for 1 h to allow one round of retrograde transport form the Golgi to the ER and then fixed.

STED sample preparation. Normal human lung fibroblasts (NHLF; Lonza) were transduced with lentiviral particles coding for ARF1 WT, ARF1 R99C or empty vector. 48 h later, the samples were washed with PBS and fixed in 4% paraformaldehyde solution (PFA) for 20 min at RT. Next, the cells were permeabilized and unspecific binding was blocked by incubation with blocking solution (3% (w/v) BSA and 0.3% (v/v) Triton X-100 in PBS) for 2 h at RT. The samples were incubated overnight at 4°C with 1 µg/ml of the primary antibodies rabbit anti-GM130 (Cell Signaling) and mouse anti-STING (Novus Biologicals) dissolved in diluted blocking solution (0.3% (w/v) BSA and 0.03% (v/v) Triton X-100 in PBS). After three washing steps with PBS, the samples were incubated with 1 µg/ml secondary goat anti-mouse antibody conjugated with Atto647N (Sigma-Aldrich), 1 µg/ml goat anti-rabbit antibody conjugated with Atto594 (Sigma-Aldrich) and anti-rat antibody conjugated with Alexa Fluor Plus 405 (Thermo Fisher Scientific, transfection control) dissolved in diluted blocking solution (0.3% (w/v) BSA and 0.03% (v/v) Triton X-100 in PBS) for 1 h at RT. Unbound antibodies were removed in three washing steps with PBS. For imaging, samples were kept in 2,2'-thiodiethanol (97% TDE solution in PBS, pH 7.5).

STED imaging. Images were captured with a home-built dual-color 3D-STED microscope[74]. Typically, an average power of ~ 1 µW for each excitation beam (568 nm and 633 nm, respectively) and ~ 1.5 mW for each depletion beam (710 nm and 750 nm, respectively) was used. STED images were captured at a pixel size of 20 nm and a dwell time of 300 µs with a typical peak photon number of ~ 150 counts. Images were analyzed by ImageJ (Fiji). For better visualization, a Gaussian blur of $\sigma = 1$ was applied in each channel.

EM preparation. Sample preparation was performed according to a standardized protocol[75]. HEK293T cells were cultivated on UV-sterilized 160 µm thin carbon-coated sapphire disks (Engineering Office M.) and transfected with ARF1 WT, ARF1 R99C or empty vector. 24 h later, the samples were then cryo-fixed at a pressure of 230 MPa within 30 ms using a high-pressure freezer (HPF Compact 101). The samples were freeze substituted in a medium of acetone with 0.1% uranyl acetate (UA), 0.2% osmium tetroxide (OsO4), and 5% double distilled water for improved visibility of the membranes[76]. Overnight (17h), samples were gradually warmed in an EM AFS2 (Leica Microsystems GmbH) freeze substitution device from − 90 to 0 °C. They were then left at 0 °C for 1 h and washed 3 times with acetone for 30 min each at room temperature and embedded in EPON resin (Sigma-Aldrich). For embedding, samples were incubated successively for one hour each in 33%, 50% and 67% EPON resin in acetone, then overnight in 100% EPON and polymerized for 48 h at 60 °C. By plunging the solidified specimens in liquid nitrogen, the EPON block breaks in the region of the embedded sapphire discs leaving the cells on the surface ready to be sectioned with an ultramicrotome (Ultracut UC7, Leica Microsystems GmbH).

EM imaging. For TEM imaging, 70 nm thin sections were mounted on carbon-coated Formvar films on copper grids (Plano GmbH) and imaged with a JEM-1400 TEM operating at 120 kV acceleration voltage equipped with a CCD camera (Veleta, Olympus Life Science). For STEM

tomography, 800 nm thick sections were put on glow-discharged copper grids with parallel bars (Plano GmbH), pre-treated with 10% (w/v) poly-L-lysine (Sigma-Aldrich), followed by a second coating with poly-L-lysine to attach 25 nm colloidal gold particles (AURION Immuno Gold Reagents) on both sides of the cross-sections. A series of tilted images of the sections from an angle of −72° to + 72° with an increment of 1.5° were recorded using a Jeol FEM 2100F field-emission TEM equipped with a Jeol STEM bright-field detector (Jeol Ltd) and , EM-Menu 4.0 STEM tomography software (TVIPS) at a resolution of 1024 px × 1024 px, an illumination time of 20 s, and an acceleration voltage of 200 kV. Alignment of the images with the gold particles as fiducial markers as well as 3D-reconstruction of the tilt series was done as previously described[77] using the IMOD 4.9 software[78].

EM stereology. According to the Delesse principle, stating that the volume density of an organelle or component in a tissue can be estimated by measuring the area fraction of the intersections of the component within a random section of the tissue[79], volume fractions of luminal structures and small vesicles were determined by counting grid points on predefined classes within square test fields of 16 µm2 size using the recursive grid option implemented in the open-source software JMicroVision image analysis system. Since it is not possible to evaluate the entire cell, the precondition for stereological evaluation was that the section through the cell contained centrioles. The test fields were chosen so that the centrioles were located in their centre. This ensured that only similar areas in the cell were evaluated, as the distribution of organelles may differ depending on the cell area.

Structural analysis. A model of the ARF1 crystal structure (2J59) retrieved from the Protein Data Bank (PDB) and visualised in UCSF Chimera 1.15. Only Chain A was displayed and R99C was highlighted by displaying the atom model.

Purification of ARF1, ARF1R99C and ARF1Q71L. For bacterial protein expression, soluble human ARF1 wild-type and mutants lacking its N-terminal 17 amino acids and human ARFGAP1 domain (1-136) were cloned into modified pET16 vector with N-terminal His_6-MBP-SUMO tag. *E. coli* BL21 Rosetta cells were grown at 37°C in lysogenic broth medium until the culture reached an OD_{600} of 0.4-0.5 and protein production was induced at 18°C with 0.4 mM isopropyl-β-thiogalactopyranoside for 16 hours. Harvested *E. coli* cells were resuspended in lysis buffer (20 mM HEPES pH 7.5, 400 mM NaCl, 30 mM imidazole, 10% glycerol and 1 mM β-mercaptoethanol) and lysed by sonication. Recombinant cell debris was removed by centrifugation and recombinant hARF1 proteins were purified over nickel-nitriloacetic acid (Ni-NTA) affinity chromatography and the His_6-MBP-SUMO tag was subsequently removed by addition of SENP2 protease at 4°C, followed by overnight dialysis against 20 mM HEPES pH 7.5, 250 mM NaCl and 2 mM β-mercaptoethanol. The proteins were further purified and separated from His_6-MBP-SUMO tag and protease by a HiLoad 16/600 Superdex 75 size exclusion chromatography column (Cytiva) in 20 mM HEPES pH7.5, 250 mM NaCl, 1 mM TCEP. Purified hARF1 were pooled, aliquoted and flash frozen in liquid nitrogen before stored at -80°C.

Thermal shift assay. The thermal stability of different hARF1 proteins in presence and absence of GTP was analysed by fluorescence thermal shift assays. 75 µM protein were incubated in 25 mM HEPES pH 7.5, 100 mM NaCl, 5 mM $MgCl_2$, 1 mM TCEP with or without 5 mM GTP. The fluorescence signal was detected after addition of SYPRO orange (final concentration 5x, Invitrogen) using gradient from 15°C to 95°C with 0.5°C/30s and one scan each 0.5°C in a real time thermal cycler (QuantStudio 3, Thermo Fisher Scientific). The deflection point of the curve and first derivative was calculated by Prism 9 (GraphPad).

Autophagy Reporter Assay. The autophagosome levels of HEK 293T cells stably expressing LC3B-GFP were assessed as previously[62]. HEK293T cells were transfected with Tag-RFP ARF1 WT, Tag-RFP ARF1 R99C or empty vector using PEI. 6 hours after transfection the medium was changed to reduce effects of transfection reagents on the cells. For samples that were treated with Bafilomycin A1, Bafilomycin A1 at a concentration of 625 µM was added to the medium. 24 h after treatment, the samples were detached and transferred to 96-well V-bottom plates. Treatment with 0.05% saponin in PBS and two subsequent washes with PBS were used to remove cytosolic LC3B-GFP. Fluorescence intensity of membrane-bound LC3B-GFP was measured using a Beckman-Coulter CytoFLEX with attached high-throughput sampler and set above 1000 to allow for detection of shifts in autophagosome levels in both directions (more or less autophagosomes). Intact single cells were gated using SSC-A / FSC-A and FSC-A / FSC-H respectively. Raw fluorescence-activated cell sorting (FACS) data were analysed using FlowJo 10. Median fluorescence intensity shifts of all samples were calculated by subtracting the LC3B-GFP-MFI of vector-treated samples from the ARF1 WT and ARF1 R99C samples.

Quantification and statistical analysis. Statistical analyses were performed using GraphPad PRISM 8. P-values were determined using a two-tailed Student's t test with Welch's correction or One-way ANOVA for multiple comparisons (Mann-Whitney test). Statistics on qPCRs over multiple values (Fig. 3f and Extended Data Fig. 3c-f) were performed using Two-Way ANOVA. Unless otherwise stated, data are shown as the mean of at least three biological replicates ± SEM. Significant differences are indicated as: *, $p < 0.05$; **, $p < 0.01$; ***, $p < 0.001$. Not significant differences are not indicated. Specific statistical parameters are specified in the figure legends.

Extended Data Figure legends

Extended Data Figure 1: a, Conservation of the amino acids in ARF1 (blue, conserved,; white, not conserved), with R99 highlighted in red as analysed by Consurf . **b**, Pedigrees of the four patients ascertained with a substitution at R99 of ARF1.

Extended Data Figure 2: Expression of ARF1 WT and ARF1 R99C. a, FLAG-tagged ARF1 WT, R99C, Q71L or T31N were transiently expressed in 293-Dual-hSTING-R232 reporter cells. Representative immunoblots of whole cell lysates (WCLs) showing the corresponding expression of STING and GAPDH, stained with anti-STING and anti-GAPDH. **b,** Exemplary immunoblot of WCLs of HEK293T cells transiently expressing FLAG-tagged ARF1 WT or R99C and co-expressing STING-FLAG (bottom) or empty vector (top). Blots were stained with anti-FLAG, anti-STING and anti-GAPDH. **c**, Impact of ARF1 WT or R99C expression on ISG induction in primary human normal lung fibroblasts (NHLF) as assessed by qPCR of Mx1 mRNA 72 h post transduction. IFN-β (1000 U/mL, 16 h) and cGAMP (10 µg/ml, 16 h) served as positive controls. Bars represent mean of n = 3 ± SEM (biological replicates).

Extended Data Figure 3: Depletion of mtDNA reduces ISG induction in the presence of ARF1 R99C. a, Impact of transient transfection of FLAG-tagged ARF1 WT or R99C on ISRE promoter activity in 293-Dual-hSTING-R232 cells either mock treated or treated with G140 (2.5 µg/ml, 32 h). SEAP activity was quantified 32 h post transfection and normalised to cell viability. Bars represent mean of n = 3 ± SEM (biological replicates). Lower panel: Corresponding immunoblots of WCLs stained by anti-FLAG, anti-STING and anti-GAPDH. **b**, mtDNA depletion in U2OS and U2OS-STING cells assessed by qPCR for the mitochondrial gene MT-COXII and the nuclear gene GAPDH. mtDNA depletion was induced by treating the cells with 100 µM 2',3'

dideoxycytidine (ddC) for seven to fourteen days. Bars represent mean of n = 3 ± SEM (biological replicates). **c**, Exemplary immunoblot of WCLs of U2OS and U2OS-STING cells left untreated (NT) or treated with 100 µM ddC for seven to fourteen days and subsequently stimulated with HT-DNA (2 µg/mL, 4 h) or treated with lipofectamine (Lipo) only. Blots were stained with anti-pIRF3, anti-IRF3, anti-pSTING, anti-STING and anti-cofilin. **d-f**, Impact of ARF1 WT, R99C or empty vector (EV) expression on ISG induction in U2OS and U2OS-STING cells treated with 100 µM ddC for seven to fourteen days or left untreated (NT). mRNA levels of Mx1, IFNB1 and RSAD2 were assessed by qPCR 24 h post transfection. Bars represent mean of n = 3 ± SEM (biological replicates). **g**, Impact of ARF1 WT and ARF1 R99C on autophagosome levels. HEK293T cells stably expressing eGFP-LC3b were transfected with TagRFP-ARF1 WT, TagRFP-ARF1 R99C or empty vector control. Shifts in autophagosome levels were assessed using flow cytometry. n = 4 ± SEM (biological replicates). **h**, Impact of ARF1 WT and ARF1 R99C on autophagosome levels in the presence and absence of Bafilomycin A1. HEK293T cells stably expressing eGFP-LC3b were transfected with TagRFP-ARF1 WT, TagRFP-ARF1 R99C or empty vector control. Shifts in autophagosome levels were assessed using flow cytometry. n = 4 ± SEM (biological replicates **i**, qPCR of mtDNA (MT-D-Loop) in the cytosolic fraction of ARF1 WT, R99C, Q71L and vector transfected HEK293T ATG5 KO relative to total normalized cellular mtDNA (mtDNA/nuclear DNA) using the ΔΔCT method. n = 4 ± SEM. **j**, Analysis of the mitochondrial footprint from the images shown in (**k**) using the MiNA plugin (StuartLab) for ImageJ (Fiji). Lines represent mean of n = 51-62 ± SEM (individual cells). **k**, Exemplary live cell confocal laser scanning microscopy images of HeLa cells expressing TagRFP-tagged ARF1 WT, R99C or vector control. Cells were treated with Mitotracker (1 µM) for 30 min at 37°C. Nuclei, Hoechst 33342 (blue). Scale bar, 10 µm, **l**, Exemplary immunoblot of WCLs of HEK293T cells transiently expressing ARF1 WT, R99C or vector control. Blots were stained with anti-pDRP1, anti-DRP1, anti-FLAG and anti-

GAPDH. Quantification of the band intensities for pDRP1 normalized to the band intensities of DRP1. Bars represent mean of n = 8 ± SEM (biological replicates).

Extended Data Figure 4: Characterisation of stability and dimerization of ARF1 WT and R99C. a, Coomassie stained SDS-PAGE gel of purified recombinant human ARF1 WT, Q71L and R99C proteins lacking its N-terminal 17 amino acids. **b,** Thermal shift assay of ARF1 WT, Q71L and R99C. Respective inflection temperatures are: ARF1 WT 58.3 °C; ARF1 R99C 44.4 °C; ARF1 Q71L 56.8 °C. Data are representative of two biological replicates. **c,** Immunoprecipitation (IP) of FLAG-tagged ARF1 WT and R99C by anti-FLAG-beads. HEK293T cells were transfected with empty vector, FLAG-tagged ARF1 WT or R99C (FLAG), or TagRFP-tagged ARF1 WT or R99C (TR), or with FLAG-tagged ARF1 WT and TagRFP-tagged ARF1 WT or FLAG-tagged ARF1 R99C and TagRFP-tagged ARF1 R99C (FLAG+TR). 24 h post transfection, cells were harvested and anti-FLAG IP was performed. Blots were stained with anti-RFP (TR), anti-ARF1 and anti-FLAG. **d-e,** IP of FLAG-tagged ARF1 WT and R99C by anti-FLAG-beads, from cell lysates of HEK293T cultivated in SILAC light medium or heavy medium for five passages, then transfected with empty vector, FLAG-tagged ARF1 WT or ARF1 R99C, harvested and lysed 24 h post transfection. After electrophoresis, in (**d**) western blot was performed and stained with anti-FLAG and anti-GAPDH, in (**e**) gel was stained with SDS-Gels silver staining. HC: heavy chain, LC: light chain.

Extended Data Figure 5: ARF1 mediated ERGIC morphology and retrograde transport from the ERGIC/Golgi to the ER. a, FLAG-tagged ARF1 WT and R99C were transiently expressed in HEK293T cells co-expressing STING-FLAG, ISRE-promoter controlled Firefly

luciferase and GAPDH-promoter controlled Renilla luciferase. Representative immunoblots of WCLs showing the corresponding expression of ARF1 WT, R99C, STING and GAPDH, stained with anti-FLAG and anti-GAPDH. **b,** Exemplary immunoblot of WCLs for Fig. 5c. Blots were stained with anti-FLAG and anti-GAPDH. **c,** Exemplary **c**onfocal laser scanning microscopy images of Hela cells expressing FLAG-tagged ARF1 WT, R99C, Q71L or T31N, corresponding to Fig. 5g. Cells were stained 24 h post transfection with anti-FLAG (red) and anti-ERGIC-53 (grey). Nuclei, DAPI (blue). Scale bar, 10 μm. **d,** Exemplary confocal laser scanning microscopy images of HeLa cells expressing VSVG-ts045-KDELR-eGFP (green) and indicated FLAG-tagged ARF1 mutants, corresponding to Fig. 5h. Cells were incubated at 37°C for 24 h and the different temperature shifts (37°C/32°C/40°C) as indicated. Staining with anti-FLAG (red) and anti-GM130 (grey). Nuclei, DAPI (blue). Scale bar, 10 μm.

Extended Data Figure 6: ARF1 R99C has increased localisation at the cis- and trans-Golgi. **a,** Exemplary confocal laser scanning microscopy images of STING-eGFP (green) and indicated FLAG-tagged ARF1 mutants in HeLa cells. Cells were stained 24 h post transfection with anti-FLAG (red) and anti-ERGIC-53 (grey). Nuclei, DAPI (blue). Scale bar, 10 μm, **b**, Quantification of the co-localisation of ARF1 and ERGIC-53 and **c**, STING and ERGIC-53 from the images shown in (**a**) using Pearson's correlation coefficient. Lines represent mean of n = 15-31 ± SEM (individual cells). **d,** Exemplary confocal laser scanning microscopy images of STING-eGFP (green) and indicated FLAG-tagged ARF1 mutants in HeLa cells. Cells were stained 24 h post transfection with anti-FLAG (red) and anti-TGN46 (grey). Nuclei, DAPI (blue). Scale bar, 10 μm. **e**, Quantification of the co-localisation of ARF1 and TGN46 and **f**, STING and TGN46 from the images shown in (**d**) using Pearson's correlation coefficient. Lines represent mean of n = 11-18 ± SEM (individual cells). **g,** Exemplary STED super-resolution microscopy images of NHLF cells

transduced with lentiviruses expressing indicated ARF1 constructs or empty vector. 48 h post transduction the cells were stained with anti-STING (green), anti-FLAG (not shown) and anti-GM130 (red). Only FLAG-staining positive cells are displayed. Scale bar, 5 μm.

Extended Data Figure 7: Model summarizing the involvement of ARF1 in cGAS-STING signal triggering and termination.

Supplementary table 1: Molecular data relating to ARF1*

Patient	Nucleotide	Amino acid	Inheritance	gnomAD	SIFT / Polyphen2 / MutationTaster
1	c.295C>T	p.(Arg99Cys)	De novo	0	Deleterious / Probably damaging / Deleterious
3	c.295C>T	p.(Arg99Cys)	De novo	0	Deleterious / Probably damaging / Deleterious
4	c.295C>T	p.(Arg99Cys)	Mother wild-type; paternal DNA not available	0	Deleterious / Probably damaging / Deleterious
2	c.296G>A	p.(Arg99His)	De novo	0	Deleterious / Probably damaging / Deleterious

Supplementary table 2: SILAC data

Supplementary table 3: PantherDB GO term Analysis

Supplementary information

Please contact the corresponding authors to request access to this information.

Figure 1

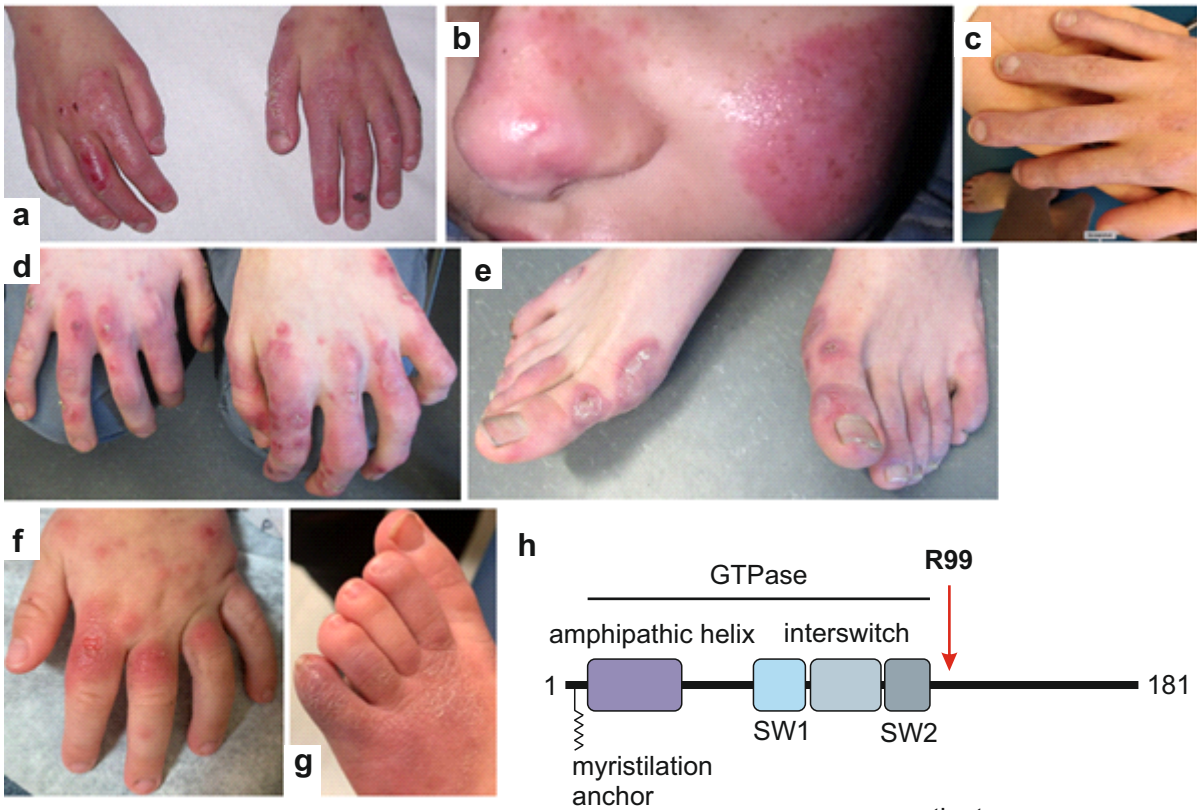

Figure 2

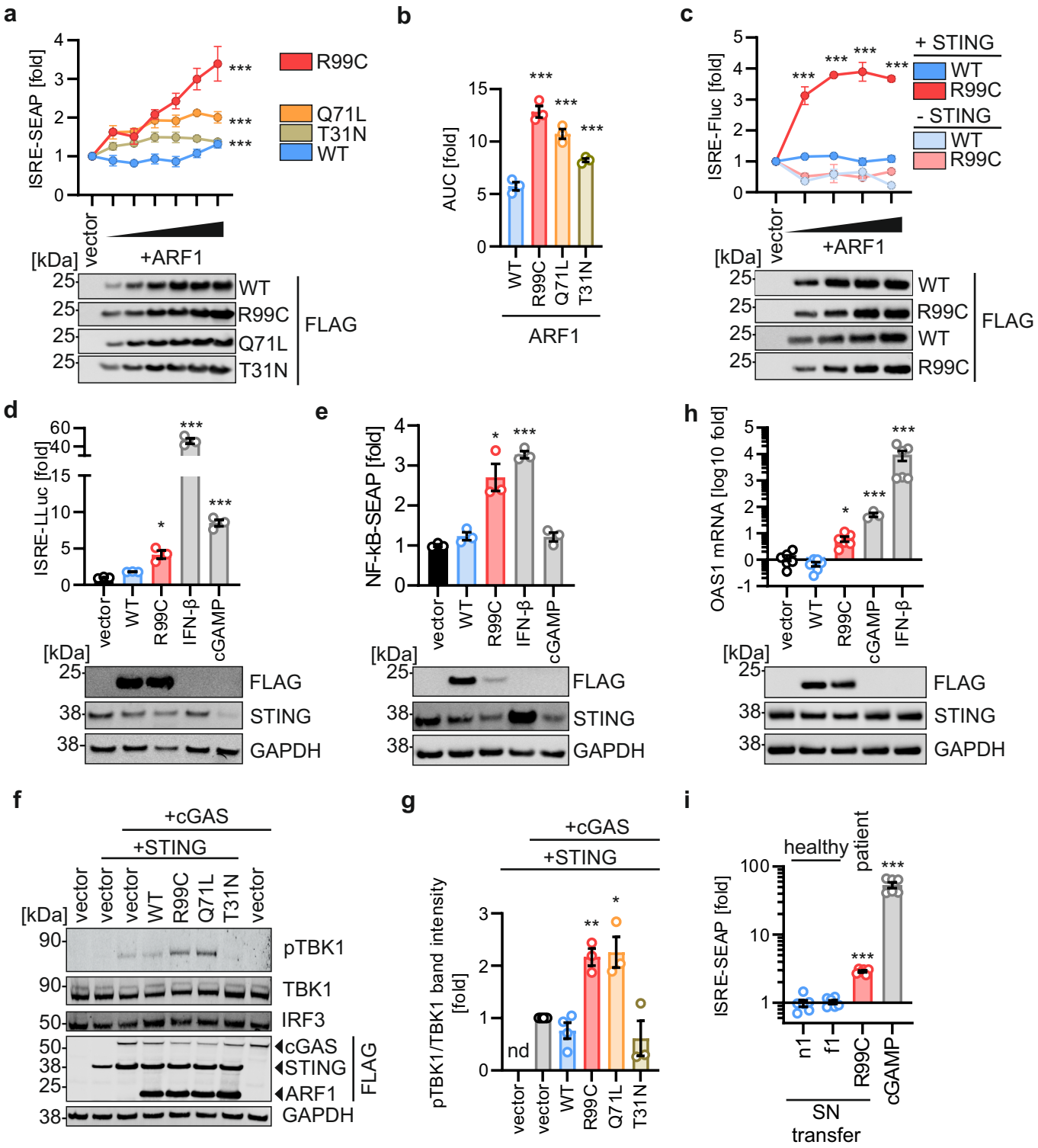

Figure 3

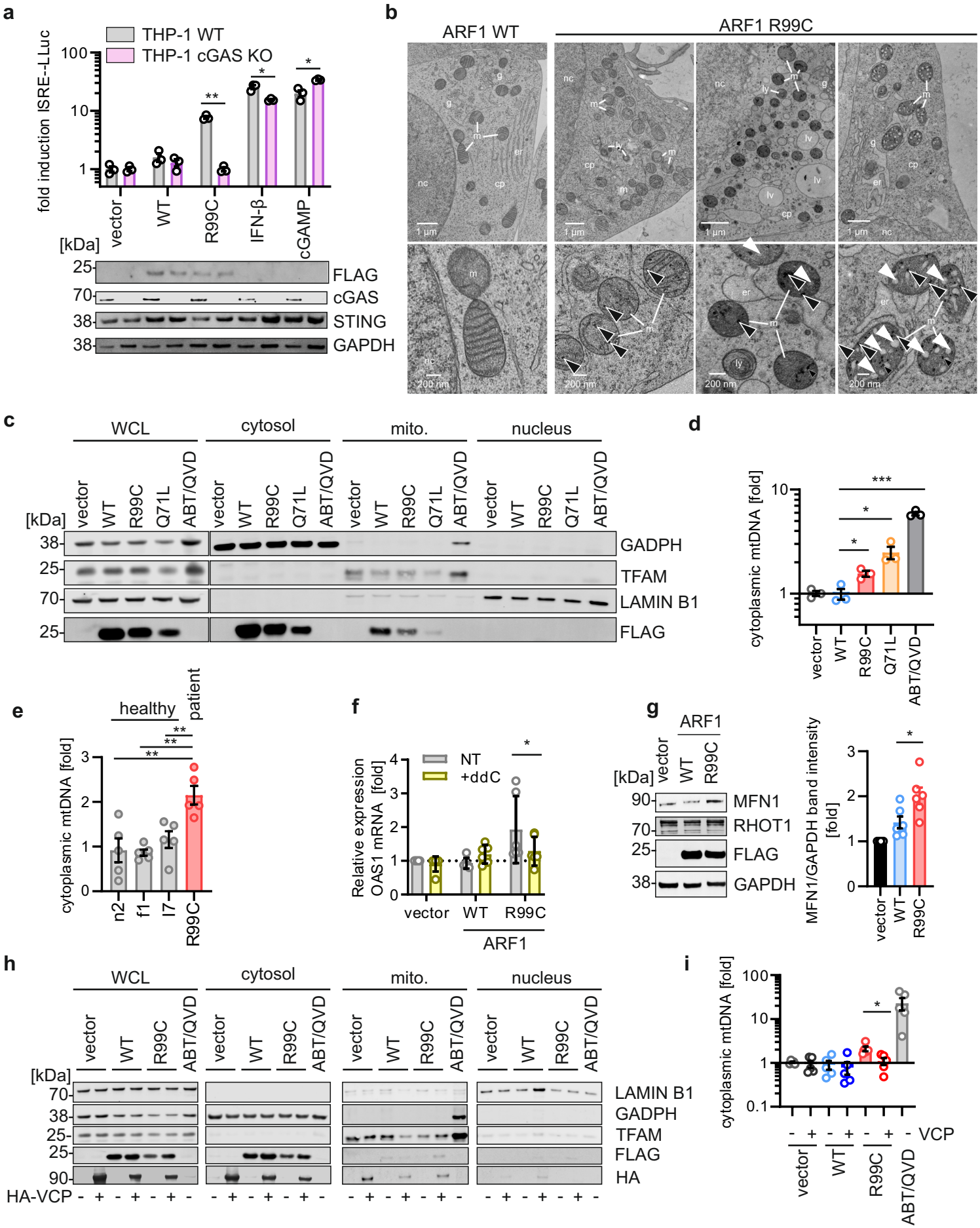

Figure 4

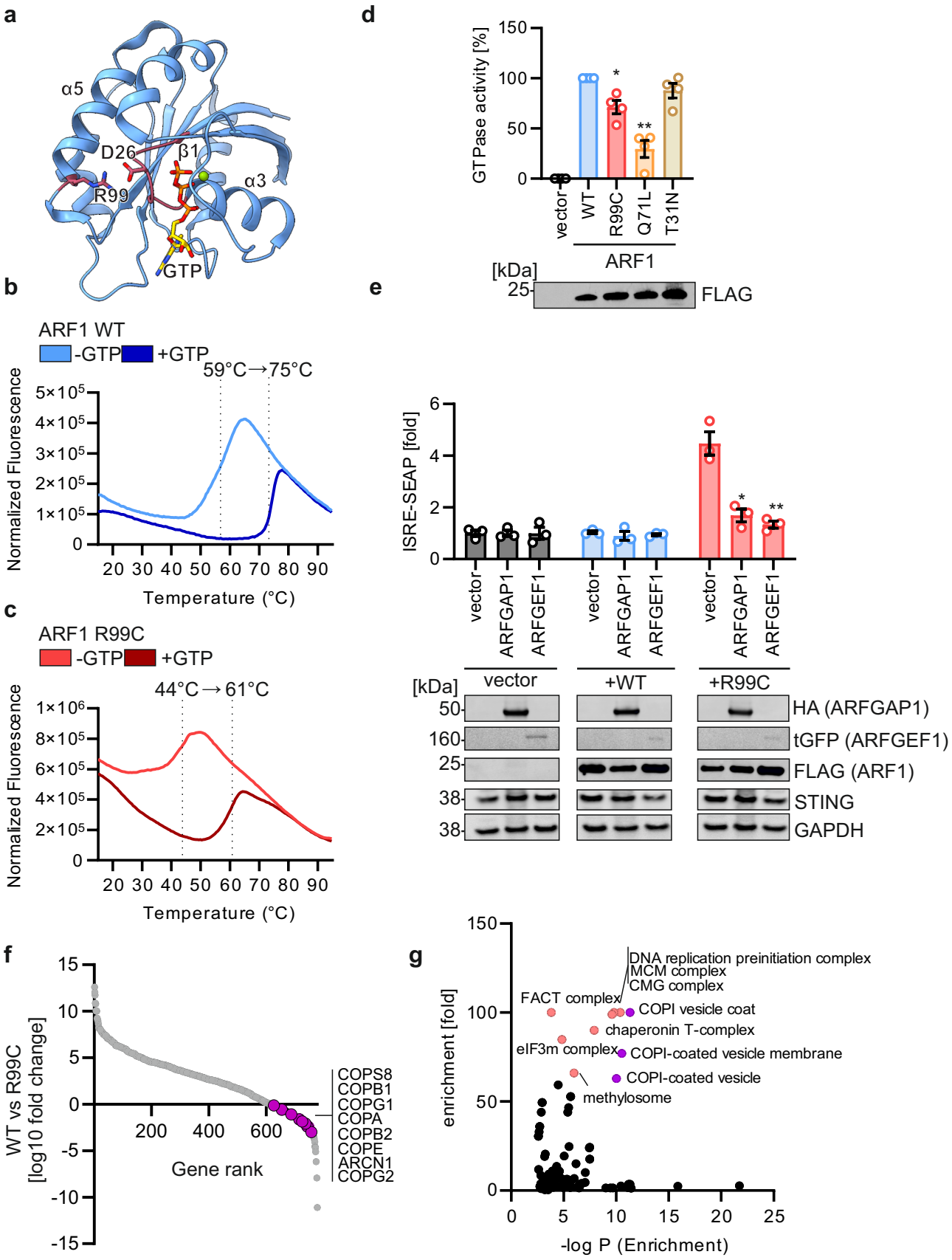

Figure 5

Hirschenberger et al.

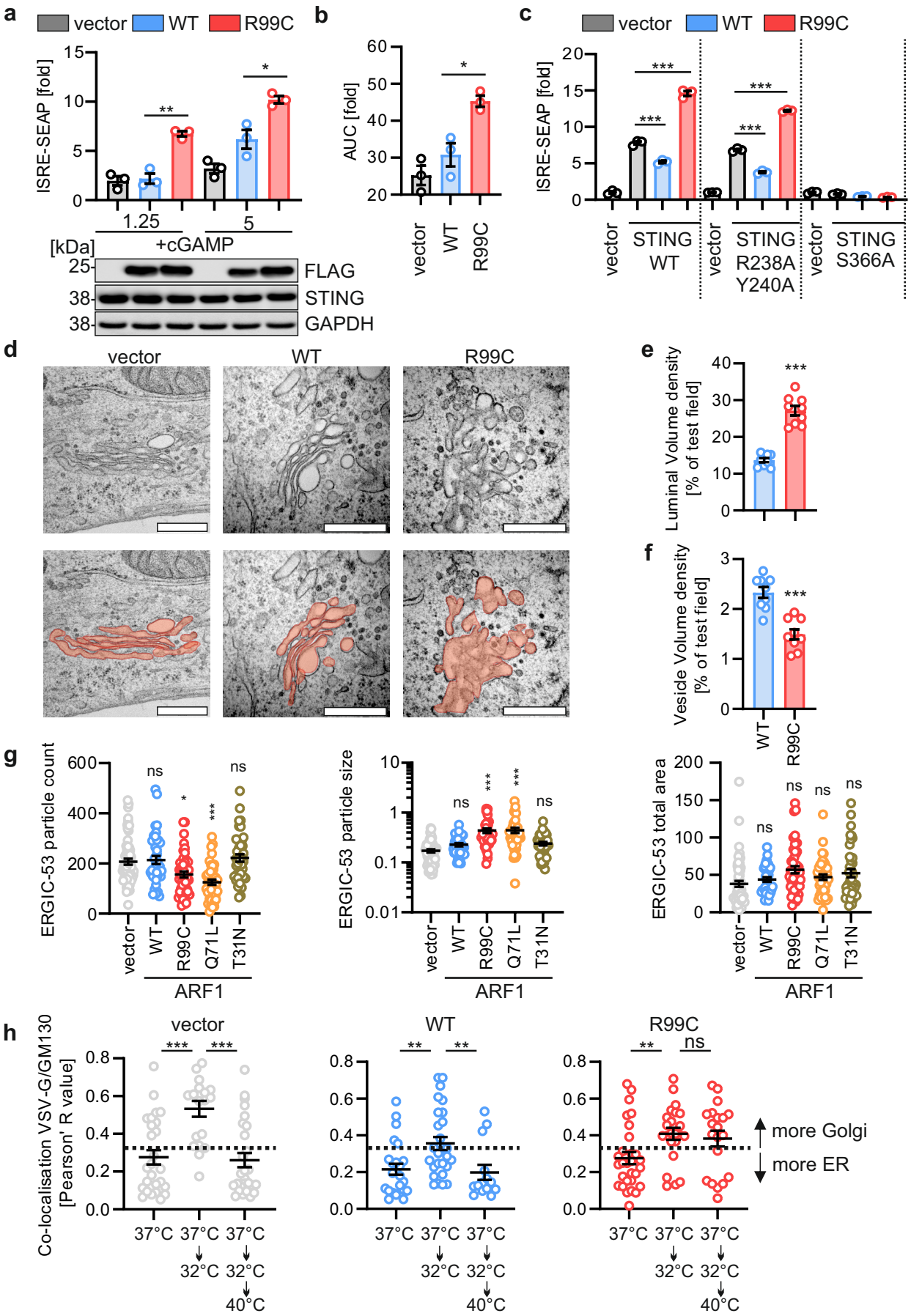

Figure 6

Hirschenberger et al.